Received: 22 October 2018 | Revised: 18 January 2019 | Accepted: 6 February 2019

DOI: 10.1111/bre.12346

ORIGINAL ARTICLE

WILEY Basin Research IAS EAGE

Miocene to Quaternary basin evolution at the southeastern Andean Plateau (Puna) margin (ca. 24°S lat, Northwestern Argentina)

Heiko Pingel[1] | **Ricardo N. Alonso**[2] | **Uwe Altenberger**[1] | **John Cottle**[3] | **Manfred R. Strecker**[1]

[1]Institute of Geosciences, Potsdam University, Potsdam, Germany

[2]Departamento de Geología, Universidad Nacional de Salta, Salta, Argentina

[3]Department of Earth Science and Earth Research Institute, University of California, Santa Barbara, California

Correspondence
Heiko Pingel, Institute of Geosciences, Potsdam University, Potsdam, Germany.
Email: heiko.pingel@geo.uni-potsdam.de

Abstract

The Andean Plateau of NW Argentina is a prominent example of a high-elevation orogenic plateau characterized by internal drainage, arid to hyper-arid climatic conditions and a compressional basin-and-range morphology comprising thick sedimentary basins. However, the development of the plateau as a geomorphic entity is not well understood. Enhanced orographic rainout along the eastern, windward plateau flank causes reduced fluvial run-off and thus subdued surface-process rates in the arid hinterland. Despite this, many Puna basins document a complex history of fluvial processes that have transformed the landscape from aggrading basins with coalescing alluvial fans to the formation of multiple fluvial terraces that are now abandoned. Here, we present data from the San Antonio de los Cobres (SAC) area, a sub-catchment of the Salinas Grandes Basin located on the eastern Puna Plateau bordering the externally drained Eastern Cordillera. Our data include: (a) new radiometric U-Pb zircon data from intercalated volcanic ash layers and detrital zircons from sedimentary key horizons; (b) sedimentary and geochemical provenance indicators; (c) river profile analysis; and (d) palaeo-landscape reconstruction to assess aggradation, incision and basin connectivity. Our results suggest that the eastern Puna margin evolved from a structurally controlled intermontane basin during the Middle Miocene, similar to intermontane basins in the Mio-Pliocene Eastern Cordillera and the broken Andean foreland. Our refined basin stratigraphy implies that sedimentation continued during the Late Mio-Pliocene and the Quaternary, after which the SAC area was subjected to basin incision and excavation of the sedimentary fill. Because this incision is unrelated to baselevel changes and tectonic processes, and is similar in timing to the onset of basin fill and excavation cycles of intermontane basins in the adjacent Eastern Cordillera, we suspect a regional climatic driver, triggered by the Mid-Pleistocene Climate Transition, caused the present-day morphology. Our observations suggest that lateral orogenic growth, aridification of orogenic interiors, and protracted plateau sedimentation are all part of a complex process chain necessary to establish and maintain geomorphic characteristics of orogenic plateaus in tectonically active mountain belts.

KEYWORDS
Andean Plateau, NW Argentina, Puna, river incision, sediment routing, surface processes

1 | INTRODUCTION

The world's orogenic plateaus have many unifying geological, geomorphic and climatic similarities. Despite having evolved in different geodynamic settings, all of the Cenozoic plateaus are characterized by steep relief along their margins (Fielding, Isacks, Barazangi, & Duncan, 1994; Masek, Isacks, Gubbels, & Fielding, 1994) and their far-reaching impact on atmospheric circulation. This in turn causes highly asymmetric precipitation patterns, run-off and erosional capacity across the plateau – from humid, windward flanks with fluvial connectivity with the foreland to arid, internally drained leeward interiors behind the plateau-bounding ranges (Allen, Saville, Blanc, Talebian, & Nissen, 2013; Ballato et al., 2013; Bookhagen & Burbank, 2006; Bookhagen & Strecker, 2008, 2012).

In these settings, the arid plateau sectors often develop because of the synergy between the wholesale or successive tectonic plateau uplift and mountain ranges that straddle the high-elevation sectors and were once part of a foreland depositional environment (Sobel, Hilley, & Strecker, 2003). Over time, this incorporation of foreland areas into a compressional basin-and-range topography of the developing plateau realm generates intermontane sedimentary basins that transform into areas with gentle slopes and reduced relief contrasts (Carroll, Graham, & Smith, 2010; Walker, Ramsey, & Jackson, 2011). If internal drainage conditions are sustained over timescales of several 10^5 to 10^6 years, such basins may attain thick sedimentary fills, become overfilled and ultimately coalesce, which further reduces relief contrasts within the evolving plateau topography (Alonso et al., 2006; Heidarzadeh, Ballato, Hassanzadeh, Ghassemi, & Strecker, 2017; Liu-Zeng, Tapponnier, Gaudemer, & Ding, 2008; Métivier, Gaudemer, Tapponnier, & Meyer, 1998; Strecker et al., 2007).

Miocene to present-day plateau building processes in the region of the Andean Plateau illustrate different stages in the attainment of low-relief topography, basin filling and coalescence. The northern Andean Plateau, the Bolivian Altiplano, comprises a morphologically mature plateau characterized by extensive, gently sloping and partly overfilled basins; however, in this environment thick sedimentary fills of the coalesced Altiplano basins do not allow for a rigorous outcrop-based analysis of the different processes that ultimately caused this topography. In contrast, the southern Andean Plateau, the Argentine Puna, is much more compartmentalized into smaller, often deformed basins, where exposed sedimentary units and intercalated volcanic units allow for a better assessment of the processes that shaped this high-elevation environment.

Highlights

- U-Pb dating of detrital zircons and tuffs refines stratigraphy of the San Antonio area (NE Puna Plateau)
- Field relations and 3D-surface reconstruction of fluvial terraces imply km^3-scale excavation since ca. 800 ka
- Coeval sedimentary changes in adjacent basins suggest causal link with conditions following the Mid-Pleistocene Climate Transition
- Plateau formation seems to result from surface uplift, orographic-induced aridification and associated effects

The Puna Plateau of the southern Central Andes of NW Argentina is largely internally drained and characterized by arid climatic conditions, with average rainfall amounts of <200 mm/year (Bookhagen & Strecker, 2008). In a closed-drainage setting such as the Puna, sediment transport should merely cause a redistribution of eroded sediment volumes between depositional centres, and subsequently lead to relief reduction as a consequence of protracted sediment storage. However, many of the coalesced basins in the Puna Plateau record a complex history of large-scale, fluvially driven surface processes that have reshaped the basin landscape, resulting in incised and abandoned fluvial terraces and alluvial fan surfaces. This is intriguing, because present-day climatic conditions on the plateau do not allow for voluminous fluvial sediment transport (Bookhagen & Strecker, 2012). The phenomenon of multiple terrace and fan surfaces provides the basis for an important question as to which processes were responsible for past forcing of aggradation, incision and redistribution of sediments in the sedimentary basins of the southern Andean Plateau.

Here, we focus on the San Antonio de los Cobres (SAC) sub-basin, which is connected with the Salinas Grandes Basin of the northeastern Puna Plateau (Figure 1). The present-day morphology of the SAC area is characterized by an extensive fluvial terrace system that has been cut into Mio-Pleistocene sedimentary basin fill. Sediment redistribution in adjacent basins, such as in the Pastos Chicos Basin (Figure 1), may have been caused by overspill and headward incision. Since this is not the case in the SAC area, this basin lends itself to

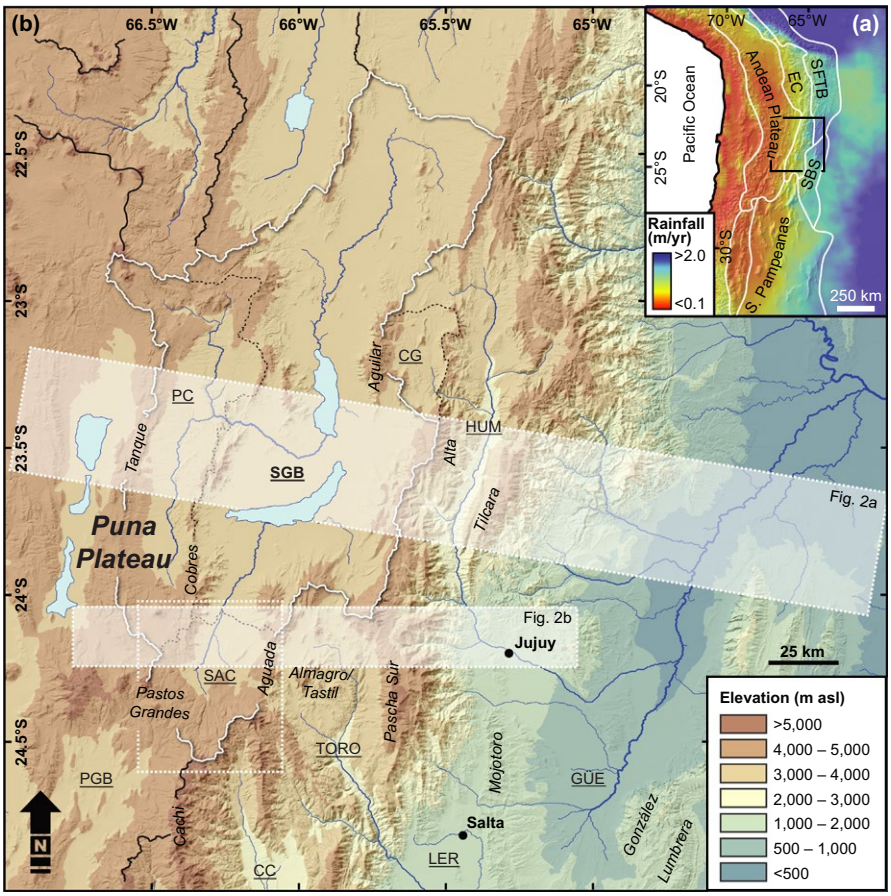

FIGURE 1 (a) Rainfall distribution and morphotectonic provinces of the South American Central Andes highlighting orographic effects of high topography on easterly moisture transport. (b) Topographic overview map showing the location of the studied San Antonio de los Cobres area (white box) in the context of a sub-catchment of the greater Salinas Grandes catchment (white outline) on the Puna Plateau in NW Argentina. Shaded rectangles delineate the areas of swath profiles shown in Figure 2. SAC–San Antonio de los Cobres area; PC-Pastos Chicos Basin; CG-Casa Grande Basin; TORO-Quebrada del Toro Basin; HUM-Humahuaca Basin; CC-Valles Calchaquíes; PGB-Pastos Grandes Basin; LER-Lerma Basin; GÜE-Güemes Basin

study of the relative roles of tectonics and climate in long-term sediment filling and incision processes. We contextualize these observations with respect to models of lateral plateau migration and extension of the plateau area during the general eastward migration of Andean deformation and increasing aridification in the course of orographic barrier uplift.

We present nine new U-Pb zircon ages from volcanic ash deposits intercalated in the Mio-Pliocene strata of the SAC area to constrain the deposition and deformation history of the eastern Puna Plateau margin. In addition, we provide two new detrital zircon maximum depositional age estimates from a ubiquitous Quaternary Black Sand and geochemical data of its components to reconstruct provenance and timing of the deposition of this important marker bed. Finally, we reconstruct the palaeo-landscape of the SAC area prior to the final episode of incision during the Pleistocene, which helps to better understand surface processes and their rates on longer timescales in this part of the Andes.

2 | GEOLOGICAL AND CLIMATIC SETTING

Due to its latitudinal extent and extensive high elevations, the Central Andes constitute a first-order topographic barrier to atmospheric circulation, resulting in extreme across-strike gradients in moisture availability (Bianchi & Yañez, 1992; Bookhagen & Strecker, 2008). For example, in NW Argentina, the eastern flanks and low-elevation foreland areas of the Central Andes receive rainfall in excess of 2,000 mm/year (Figure 1) and are characterized by dense vegetation cover. In contrast, orogen-interior regions, such as the high-elevation Puna Plateau to the west and the topographically intermediate transitional intermontane basins along its eastern margin, receive progressively less rainfall (<200 mm/year, Figure 2) and are characterized by increasingly arid conditions in a westward direction (Bianchi & Yañez, 1992; Bookhagen & Strecker, 2008). This contrast in the spatial distribution and amount of rainfall is accompanied by a strong gradient in fluvial run-off and the efficiency of surface processes, which results in very subdued surface-process rates in the internally drained, low-relief plateau (Bookhagen & Strecker, 2012).

The San Antonio de los Cobres catchment area is located on the northeastern Puna Plateau between 24 and 24.5°S lat at a mean elevation of ca. 4,200 m (3,600–5,750 m; Figures 1 and 3). With the exception of its northern outlet, this sub-basin is enclosed by high-elevation basement ranges and volcanic centres. To the west, the study area is confined by the approximately north-south oriented, reverse-fault-bounded Sierra de los Cobres that separates the SAC area from the adjacent Pastos Chicos Basin. To the south, the area is bordered

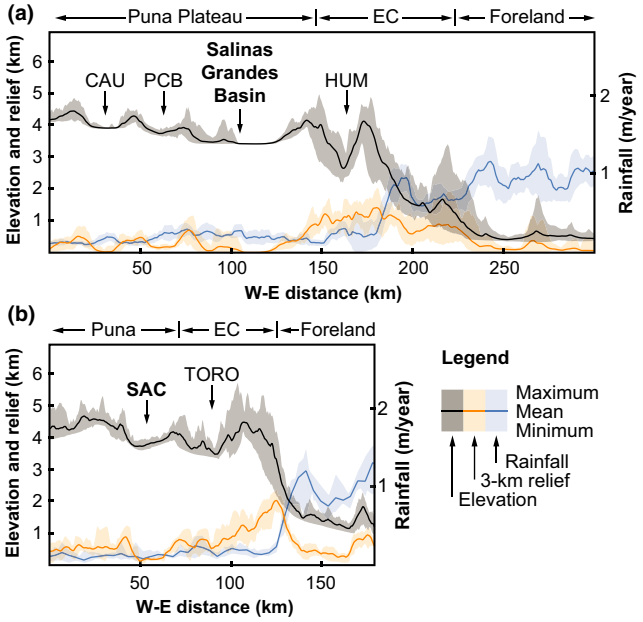

FIGURE 2 Swath profiles highlighting gradients in elevation, rainfall and 3-km radius relief across the eastern Andean margin. Note, the contrast in relief and rainfall between the internally drained Puna Plateau and the Eastern Cordillera, associated with drainage conditions and orographic rainout respectively. For location see Figure 1

by the Sierra de los Pastos Grandes – a WNW-oriented chain of Mio-Pliocene volcanic centres (e.g. Agua Caliente, Aspero and Abra de Acay), and the northern tip of the Cachi Range basement uplift. Finally, basement ranges of the Eastern Cordillera, such as the Crestón Alto la Aguada, constitute the eastern border that separates the Puna from the presently externally drained Quebrada del Toro (Figures 1 and 3).

Following Cretaceous-Early Palaeogene extension and thermal subsidence, associated with the deposition of the Salta Group (Marquillas, del Papa, & Sabino, 2005), sedimentation in the region of the present-day SAC area resumed during the Late Eocene with sands and conglomeratic redbeds of the Casa Grande Formation (Hongn et al., 2007; Montero-López, del Papa, Hongn, Strecker, & Aramayo, 2016; Steinmetz & Galli, 2015). These beds were most likely deposited in a fluvially connected, but largely broken foreland basin related to spatially distributed surface uplifts that mark the onset of Andean shortening in an area that includes the present-day eastern Puna Plateau margin (del Papa et al., 2013; Hongn et al., 2007; Jordan & Alonso, 1987; Montero-López et al., 2016; Payrola, Powell, del Papa, & Hongn, 2009; Steinmetz & Galli, 2015). Further insights regarding the earlier morphotectonic evolution of the region comes from thermochronological and tectono-sedimentary studies, which have shown that most of the SAC-bounding ranges experienced exhumation, deformation, and presumably to some degree surface uplift during Middle Eocene to Early Oligocene times (Andriessen & Reutter, 1994; Deeken et al., 2006; del Papa et al., 2013; Hongn et al., 2007; Letcher, 2007; Payrola et al., 2009; Pearson et al., 2013; 2012).

In the Miocene, this broken foreland became further compartmentalized, which resulted in the structural separation from the present externally drained areas of the Andes to the east, basin filling and surface uplift of those areas that now constitute the internally drained, high-elevation eastern Puna Plateau. As a consequence of this range uplift and the accompanying orographic effects impacting easterly, moisture-laden winds, the SAC area receives only about 120 mm of rainfall per year with peak rainfall in austral summer (December to February). Estimates of cosmogenic nuclide-derived basin-wide erosion rates in areas nearby are on the order of 0.02 mm/year or less (Bookhagen & Strecker, 2012). In contrast, surface processes from the adjacent Eastern Cordillera and the foreland are an order of magnitude higher (Bookhagen & Strecker, 2012; Schildgen et al., 2016).

An areally extensive fluvial, conglomerate-covered terrace system cut into Mio-Pleistocene sediments characterize the present-day morphology of the study area, which is drained by the San Antonio River into the Salinas Grandes sedimentary basin to the north, at an altitude of ca. 3,400 m. This basin constitutes the depositional centre of one of the largest internally drained catchments on the Argentine Puna Plateau (ca. 17,000 km^2, Figure 1) and contains a large salt-pan rich in boron and lithium.

3 | CENOZOIC STRATIGRAPHY

The Cenozoic record of the SAC area contains a less than 1-km-thick sequence of fluvial, alluvial and volcaniclastic deposits that are key to understanding the palaeoenvironmental evolution of the northeastern Puna Plateau at this latitude (Figure 3; Supporting information Figure S2). These units unconformably overlie basement lithologies of Neoproterozoic to Early Cambrian metasediments of the Puncoviscana Formation (Omarini, 1983; Turner, 1960) and Ordovician intrusive rocks grouped into the Faja Eruptiva de la Puna Oriental (or Faja Eruptiva, Mendez, Navarini, Plaza, & Viera, 1973). At the eastern SAC margin, deformed continental clastic rocks of the rift-related Cretaceous-Palaeogene Salta Group crop out in the footwall of the reverse Muñano Fault. Minor outcrops of associated post-rift sequences (Balbuena and Santa Bárbara subgroups) are exposed in the centre of the SAC area (Blasco & Zappettini, 1996), where a major N-S oriented and possibly fault-related anticline exhumed Palaeogene to Neogene strata (Figure 6).

Where the Los Patos River has cut through this structure, that is, at the Corte Blanco locality (Figs. 3 and 6), the folded strata comprise eastward-tilted beds of the Santa Bárbara Subgroup (Lumbrera and Maíz Gordo formations) that are unconformably overlain by yellow to brown-coloured cobble

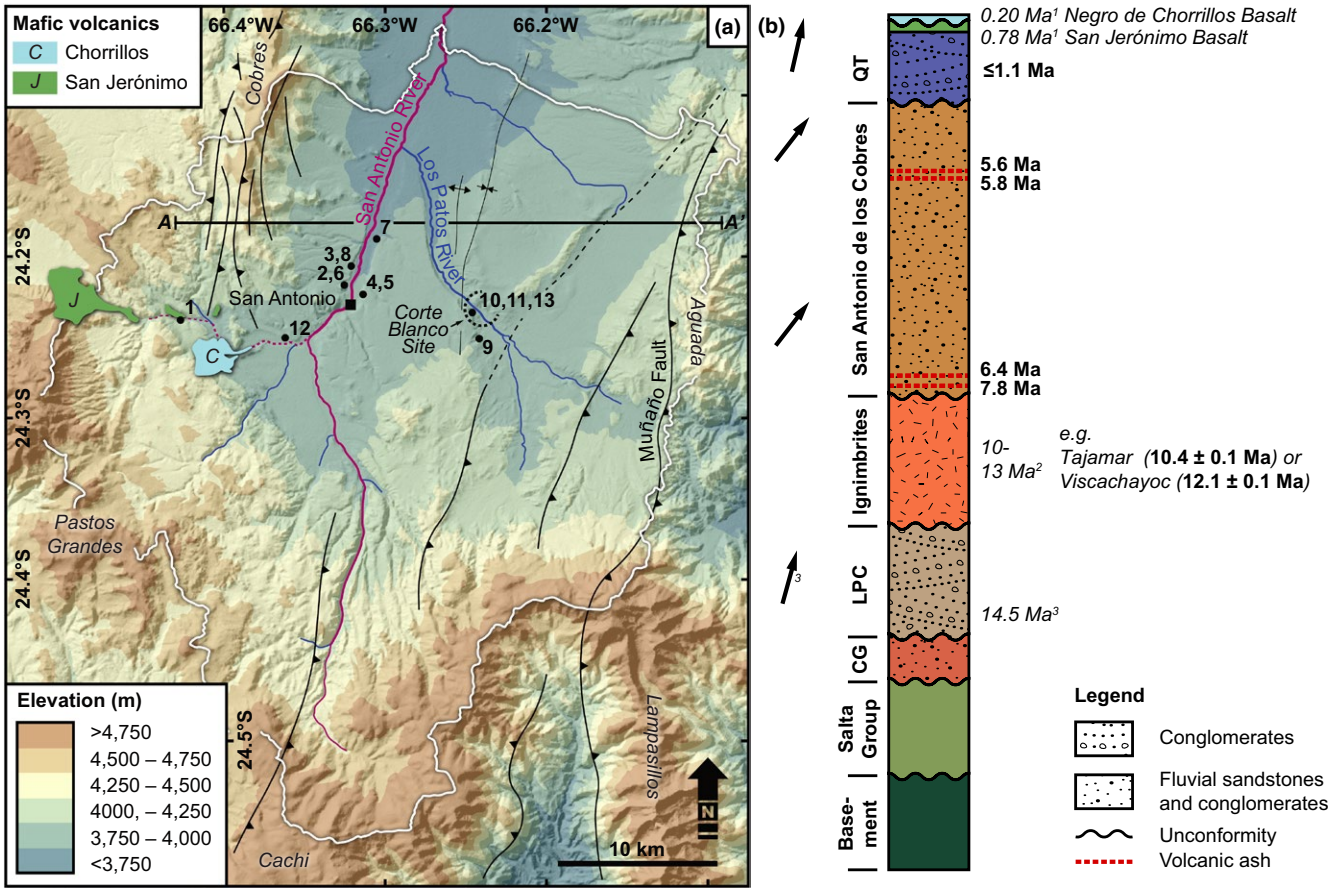

FIGURE 3 (a) Topographic and structural map of the SAC area with main drainage system and major reverse faults. Numbered dots show the location of sample sites and correspond to sample number in Table 1. Geological cross section through A–A′ is shown in Figure 4. (b) Simplified stratigraphic profile (not to scale) showing the existing strata, published and own age estimates and palaeoflow data. [1]Aquater (1980); [2]Petrinovic et al. (1999); [3]del Papa and Petrinovic (2017); If not otherwise indicated data is from this study

to boulder conglomerates and fanglomerates of the Los Patos Conglomerate (Ramos, 1970). More recently, these conglomerates have been interpreted to have been emplaced in a transpressional setting during regional tectonic and volcanic activity, associated with strike-slip deformation of the WNW-oriented Calama-Olacapato-El Toro (COT) fault system (del Papa & Petrinovic, 2017). A maximum depositional age of the Los Patos Formation of 14.5 ± 0.5 Ma is constrained by U-Pb zircon dating of re-transported volcanic clasts. Here, at the Corte Blanco locality, the middle Miocene Viscachayoc Ignimbrite (13.0 ± 0.3 Ma and 12.4 ± 0.1 Ma, Petrinovic et al., 1999 and this study) unconformably covers older units. Moreover, between at least 13–10 Ma, volcanic activity in the northeastern Puna led to the eruption and emplacement of large volumes of ignimbrites in the SAC area (Petrinovic et al., 1999, 2010; for example, Tajamar and Morro ignimbrites, Petrinovic et al., 1999, 2010).

Following a period of local deformation and erosion, the SAC area was unconformably filled with an at least 150-m-thick sequence of mainly fluvial, alluvial and volcaniclastic deposits. These sediments have previously been grouped into Pleistocene-Holocene, tuff-bearing and terrace-forming fanglomerates (Blasco & Zappettini, 1996). However, in this study, we show that this stratigraphic unit, that we refer to as the San Antonio de los Cobres Formation (*nomen novum*), is in fact Late Mio-Pliocene in age. Based on our field observations the San Antonio de los Cobres Formation consists of mainly dark-toned, fine- to coarse-grained sands that frequently interbedded with imbricated gravel to pebble conglomerates (Supporting information Figure S2 and Table S8) and occasional volcanic ash deposits.

All of these units are unconformably covered by Quaternary sands and cobble to boulder conglomerates. An integral part of these deposits is a mostly black, sandy deposit, which had previously been assigned a volcanic origin (Seggiaro, Guzmán, Pereyra, Coppolecchia, & Cegarra, 2016). Following these depositional events, a major episode of incision led to the dissection of the landscape and the abandonment of terrace surfaces as high as 100 m above the present-day course of the San Antonio River (Figures 4 and 5).

Finally, the SAC area was affected by Pleistocene shoshonitic–andesitic, monogenetic volcanism that caused the

TABLE 1 Summary of geochronological results

No.	Sample ID	Lithology	Latitude (°S)	Longitude (°W)	Elevation (m asl)	Age (Ma)	Error (Ma)	MSWD	Grains	GRT[c]	Method
1	SA-291016-1	Sand	24.238	66.426	4,020	1.13	±0.25	–	1/120		U-Pb[a] DZ
2	SA-261016-2	Sand	24.216	66.324	3,814	1.72	±0.10	–	1/120		U-Pb[a] DZ
3	SA-140316-1	Tuff	24.202	66.32	3,800	5.49	±0.05	1.74	11/40		U-Pb
4	SA-110313-2	Tuff	24.218	66.313	3,800	5.60	±0.07	–	1/40		U-Pb[a]
5	SA-110313-1	Tuff	24.218	66.313	3,800	5.75	±0.06	1.73	30/49		U-Pb
6	SA-261016-3	Tuff	24.216	66.326	3,784	6.93	±0.05	–	19/49	x	U-Pb[a]
7	SA-251016-1	Tuff	24.181	66.306	3,717	7.33	±0.03	2.00	26/40	x	U-Pb
8	SA-140316-2	Tuff	24.203	66.32	3,790	7.30	±0.50	–	–	x	[b]
9	SA-261016-1	Tuff	24.251	66.245	3,970	7.30	±0.50	–	–	x	[b]
10	QT-100313-4	Tuff	24.226	66.254	3,835	6.38	±0.07	–	1/29		U-Pb[a]
11	CB-180313-1	Tuff	24.228	66.253	3,840	7.77	±0.06	1.95	5/35		U-Pb
12	SA-261016-4	Ignimbrite	24.25	66.361	3,829	10.36	±0.07	1.99	23/44		U-Pb
13	CB-190316-1	Ignimbrite	24.231	66.251	3,910	12.05	±0.13	1.98	43/99		U-Pb

[a]U-Pb zircon maximum depositional age. [b]Age correlation based on mineral content. [c]GRT-Garnet-bearing; DZ-detrital zircon.

formation of the San Jerónimo (0.78 Ma) and Negro de Chorrillos (0.2 Ma) volcanoes (Aquater, 1980) and their associated lava flows, whose paths are important features that help to determine Pleistocene surface processes in the SAC area.

4 | METHODS

4.1 | Palaeo-landscape reconstruction

For the 3D reconstruction of the palaeotopography spanning the abandoned terrace system, we used a combination of field- and satellite-based mapping and DEM-processing tools in ArcGIS software and TopoToolbox, a Matlab-based toolset for topographic analysis (Schwanghart & Kuhn, 2010). After mapping the associated terrace surfaces, we extracted flat to gently sloping surfaces with inclinations of < 2° from NASA's Shuttle Radar Topography Mission (SRTM) Global 1-arc second data (30-m DEM). In addition to the targeted terraces, this extraction layer also contains unwanted flat areas that streams have cut into the landscape. To exclude such areas from the palaeosurface reconstruction, we generated a dense river network with minimum upstream areas of 0.1 km^2 and applied an enveloping clipping mask with a dynamic buffer radius set at 90 times the channel stream order (90 m < buffer radius < 630 m). This buffer range accounts for the downstream widening of riverbeds and ensures an optimum yield of terrace-associated pixels. Finally, the resulting raster elevation layer, containing data from surface vestiges of the fluvial terrace system, was fed into ArcGIS's TopotoRaster interpolation method to generate a hydrologically correct topography. From this palaeotopography layer, the modern topography was subtracted to obtain a volume estimate of removed sediment. Further details are provided in a Matlab script with the supplementary material.

To explore geomorphological parameters of the palaeo- and modern landscapes in 2D, we used several functions of the TopoToolbox (Schwanghart & Scherler, 2014). For example, the *streamproj* function, to generate downstream projections of un-dissected river segments based the slope-area scaling by Flint (1974). Or, the *ksn* function, to calculate normalized steepness indices (k_{sn}) along a stream network, to identify characteristic knick zones and derive information on potential tectonic perturbation or lithological controls (Kirby & Whipple, 2001, 2012).

4.2 | U-Pb zircon geochronology

Zircons were extracted using standard magnetic and heavy liquid methods, handpicked, mounted in epoxy and polished for U, Th and Pb isotope analysis using a Laser Ablation Multi-Collector Inductively Coupled Plasma Mass Spectrometer (LA-MC-ICPMS) at the University of California, Santa Barbara, USA. Due to pre-eruption residence times and/or post-eruptive sedimentary reworking, analysed grains

sometimes show a wide distribution of $^{206}Pb/^{238}U$ zircon ages. Therefore, we systematically excluded the oldest ages from the calculations of an average zircon crystallization age until near-unity values for the mean square of weighted deviates (MSWD < 2) were achieved.

U-Pb detrital zircon analyses were performed using the same instrumental setup. $^{206}Pb/^{238}U$ zircon ages were then plotted and peaks of the Kernel density estimation were analysed using the DensityPlotter software (Vermeesch, 2012).

All analytical results and further methodological information can be found in the supplementary material (Supporting information Tables S1–S5).

4.3 | Scanning electron microscopy and X-ray elemental analysis (SEM-EDS)

To determine the origin of the Quaternary Black Sand, that is, to resolve the question whether or not these sediments are the erosional product of local mafic lava flows, and thus be able to better constrain the maximum depositional age of the deposit, we used an energy-dispersive X-ray spectrometer (Oxford Instruments INCAx-act) attached to a JEOL JSM-6510 scanning electron microscope. For this purpose, mafic grains of unambiguous volcanic origin were hand-picked (Supporting information Figure S3) from a sieved sample (500–710 μm), embedded in epoxy, polished and carbon-coated. Acceleration voltage was 15 keV with a beam current of 20 nA. Counting times of 180 s for each area segment (2×10^4 to 4×10^4 μm^2) were used to analyse the composition of the volcanic clasts. Mineral analyses were achieved by 60 s counting time. The alkaline and silica compositions were then compared with published geochemical data from volcanic deposits in this part of the Puna to determine a source lithology. All analytical data can be found in the supplementary material (Supporting information Tables S6 and S7 and Figure S5).

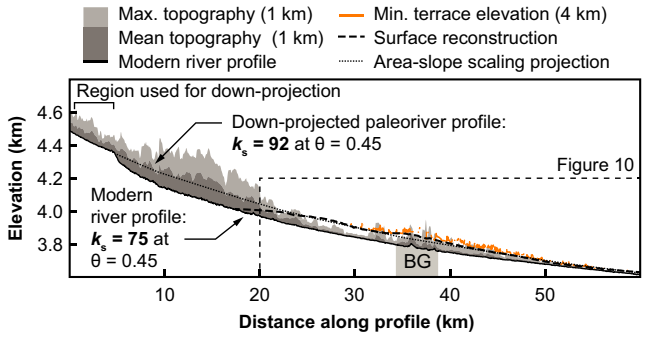

FIGURE 4 Modern river profiles of the San Antonio River (black line) with long-profile topography (shaded area, km refers to swath radius). Bold dashed line represents a projection of the reconstructed palaeosurface along the modern San Antonio River. Yellow lines represent minimum elevations along the San Antonio River of flat (<2° slope) areas associated with the mapped sections of the terrace surface. Finally, the dotted line shows a hypothetical stream profile that was projected downstream from an un-dissected section of the river at ca. 4,400 m asl. Details are discussed in the main text. BG: Basement gorge

5 | RESULTS

5.1 | Palaeo-surface reconstruction and stream-profile analysis

As expected, the reconstructed palaeosurface of the terrace system is generally in good agreement with the remnants of the abandoned fluvial terrace in the SAC area. This is for example shown in Figure 4 depicting the river-long profiles of (a) the modern San Antonio River (black line); (b) reconstructed palaeo-elevations (dashed line); and (c) minimum elevations of mapped terraces from across a 4-km swath along the profile (yellow discontinuous line). Note the match between the reconstructed surface and the mapped terrace remnants.

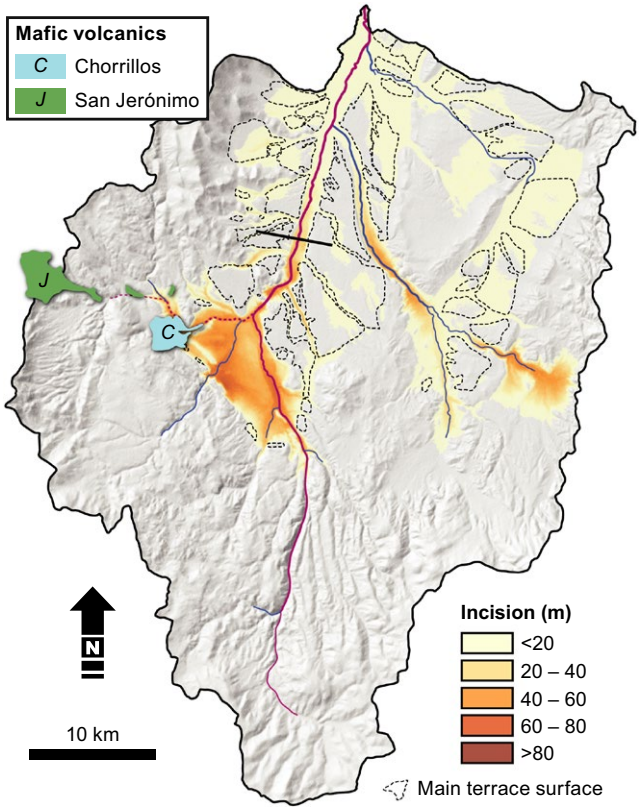

FIGURE 5 Shaded-relief map of the San Antonio de los Cobres catchment area showing the distribution of material removed since the abandonment of the main fluvial terrace between 0.78 and 0.2 Ma. Amount of incision was deduced from the residual volume between modern and reconstructed pre-incised topography. The total amount of excavated material since ca. 0.78 Ma was calculated to ca. 6.5 ± 2.0 km^3. Dashed lines outline the vestiges of the identified terrace surface in the SAC area. Black line shows the location of a topographic swath profile shown in Supporting information Figure S8

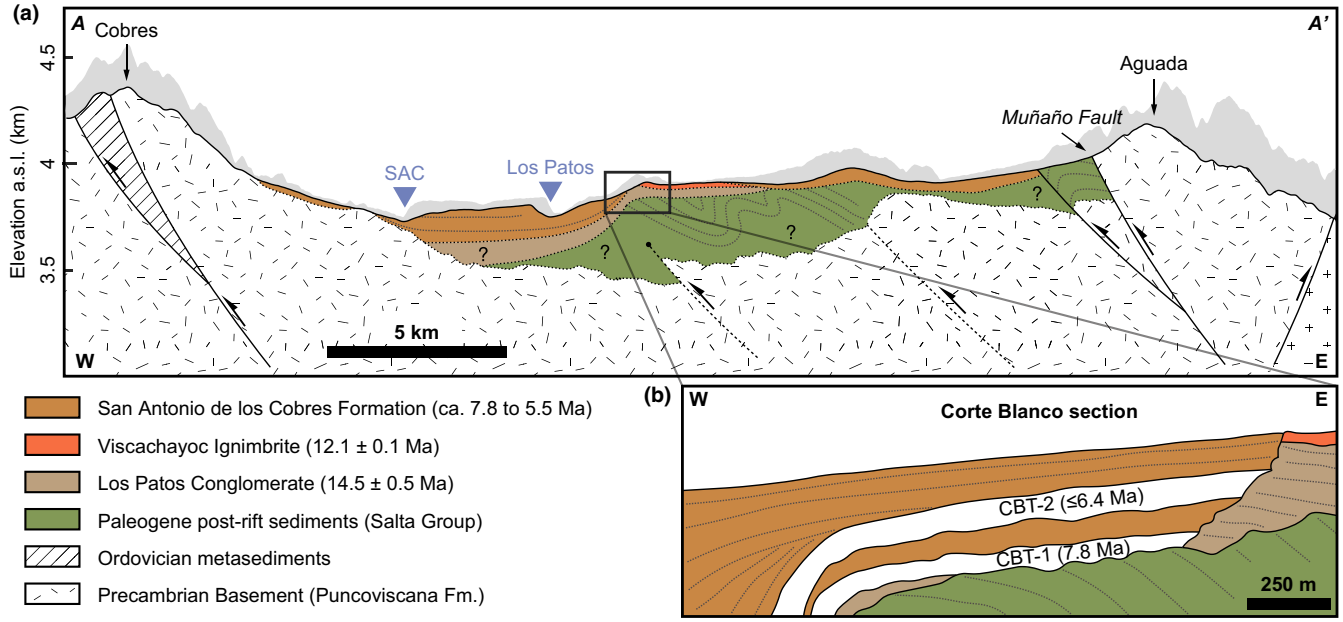

FIGURE 6 (a) Simplified W–E geological cross section showing the tectono-sedimentary setting of the SAC area and its major geological units, as deduced from field observations and the regional geological map (Blasco & Zappettini, 1996). Elevation profile is from SRTM 30 m swath profile with grey area representing the maximum elevation and the black line is the mean elevation. (b) Schematic bedding relationships at the Corte Blanco site ca. 7 km east of SAC town. Note the erosional and angular unconformities between the units and the growth strata in the Late Mio-Pliocene San Antonio de los Cobres Formation. Illustration not to scale

Two more conclusions can be drawn from the same diagram (Figure 4). First, our reconstruction clearly shows that the palaeosurface gradually converges with the modern riverbed near the basin outlet to the north. Secondly, the palaeosurface does not exceed 4,000 m in elevation, which is a clear limitation of our approach to reconstruct palaeotopography that only accounts for fluvial terrace surfaces in the basin and not the pediment surfaces in the piedmont region flanking the basin-bounding ranges.

The longitudinal profile of the modern San Antonio River has a pronounced knickpoint at ca. 4,400 m (Figure 4) above which the landscape has not been adjusted to modern drainage settings. To test whether this river section is related to the filled stage of the SAC area, we used a slope-area scaling relationship ($S = k_s A^{-\theta}$) to down-project the stream profile from this river section. A best-fit projection that meets both the observed convergence at the catchment outlet and elevations of the abandoned terrace surface was found by imposing a concavity index of $\theta = 0.45$ and resulted in an average steepness index of $k_s = 92$ (Figure 4). In contrast, the modern lower reach of the San Antonio River is less steep ($k_s = 75$), hence, river incision caused a flattening of the channel profile.

Using the reconstructed palaeosurface, the sediment volume removed from the SAC area is estimated to ca. 6.5 ± 2.0 km^3 (Figure 5). The associated uncertainty is calculated using the average misfit of 6.4 m between the measured terrace pixel elevation and the terrace pixel elevation from the generated palaeosurface. Due to the limitations described above, we are aware that this volume estimate lacks some material that has been removed at higher elevations. However, since the river incision has produced mainly narrow valleys, eroded volumes above 4,000 m are likely to be negligible.

Finally, we calculated normalized steepness indices (k_{sn}) for individual stream segments of ≥50 m^2 catchments to investigate potential spatial patterns in k_{sn}. We found that elevated k_{sn} values >150 only occur where granitic rocks of the Ordovician Faja Eruptiva or Precambrian metasediments of the Puncoviscana Formation are exposed. There appears to be no spatial correlation between elevated k_{sn} values that would suggest fault activity (Supporting information Figure S4).

5.2 | Geochronology

We analysed zircons from nine volcanic ash deposits and ignimbrite units intercalated with the sedimentary record of the SAC area using U-Pb zircon dating. Results are summarized in Table 1. The oldest sample, CB-190316-1, is from an ignimbrite exposed at the Corte Blanco site (No. 13 in Figure 3). U-Pb zircon dating yields an age of 12.05 ± 0.13 Ma, which partially agrees with the reported age of the Viscachayoc Ignimbrite (13.0 ± 0.3 Ma K-Ar biotite, Petrinovic et al., 1999). Another ignimbrite sample, located southwest of the town of San Antonio (No. 12), yielded 10.36 ± 0.07 Ma. Age and locality

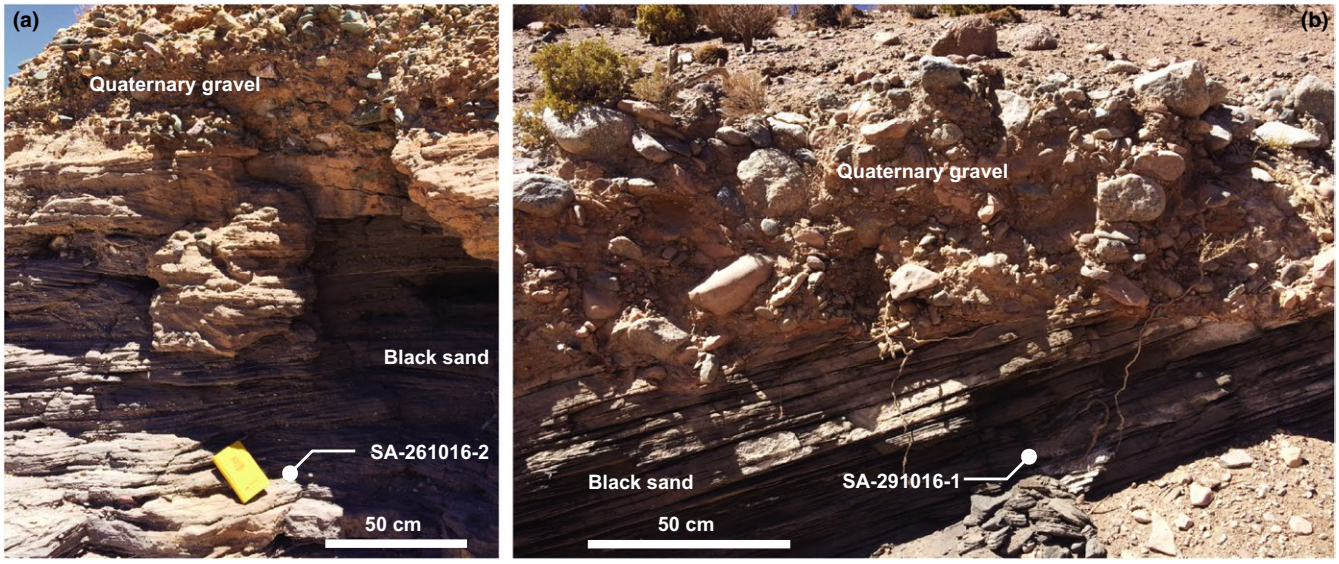

FIGURE 7 (a) Fluvial cross-beds in the Quaternary Black Sand from sampling location No. 2 overlain by Quaternary conglomerates. The detrital zircon maximum depositional age for this location is ca. 1.7 Ma (SA-261016-2, Table 1). (b) Tilted beds of the Quaternary Black Sand at location No. 1 overlain by boulder to cobble conglomerates. The detrital zircon maximum depositional age for this sample is ca. 1.1 Ma (SA-291016-1, Table 1)

suggest that this is the Tajamar Ignimbrite that erupted from the Aguas Calientes Caldera during the Miocene (ca. 10.3 Ma K/Ar, Petrinovic et al., 1999, 2010). Further U-Pb zircon ages of volcanic ash deposits within the SAC Formation provided an age range between 7.77 ± 0.06 Ma, near the basal unconformity at the Corte Blanco site (No. 11), and 5.49 ± 0.05 Ma, ca. 50–100 m higher in the succession (No. 3).

Stratigraphic correlation was performed for volcanic ash deposits that yielded characteristic, millimetre-sized idiomorphic garnet, to correlate collected samples with dated garnet-bearing ash deposits in the SAC area (No. 6 and 7). Such garnet-bearing ash deposits are, for example, SA-251016-1 and SA-261016-3, which were dated to 7.33 ± 0.03 Ma and 6.93 ± 0.14 Ma respectively. SA-251016-1 is from an outcrop along the San Antonio River (No. 7) and SA-261016-3 is from a volcanic deposit that lies unconformably above Proterozoic basement rocks at No. 6, which highlights the existence of a palaeotopography with basement exposure during the latest Miocene.

Finally, we analysed detrital zircons from two samples of Quaternary Black Sand (SA-291016-1 and SA-261016-2, Figure 7). Their youngest U-Pb ages suggest that these

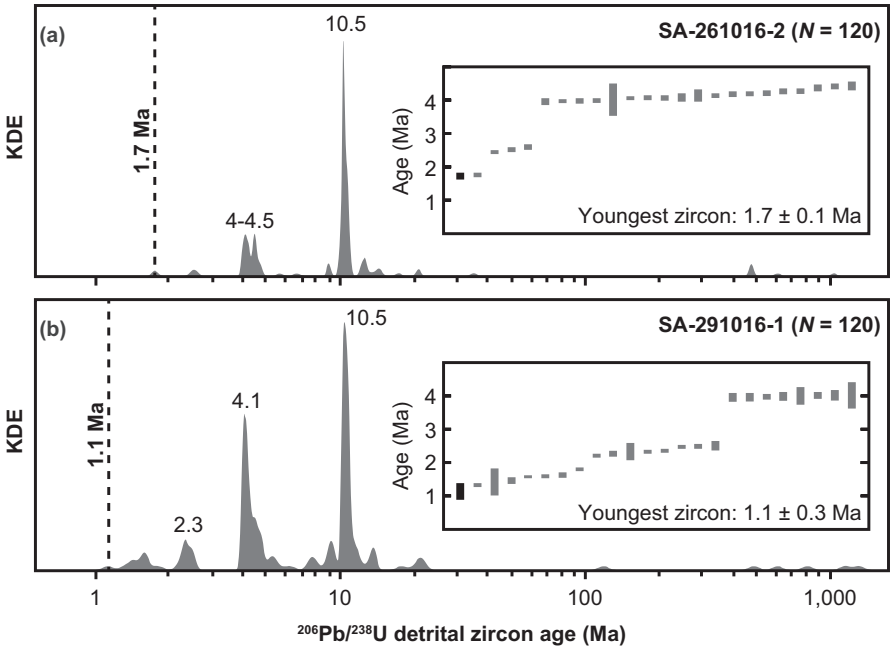

FIGURE 8 Kernel density estimate (KDE) plots for Quaternary Black Sand samples (a) SA-261016-2 and (b) SA-291016-1. Both samples equally show distinct peaks at ca. 10.5 Ma and between 4 and 4.5 Ma. Inset plots show the radiometric results from the 24 youngest zircons. Maximum depositional ages were derived from each sample's youngest zircon grain

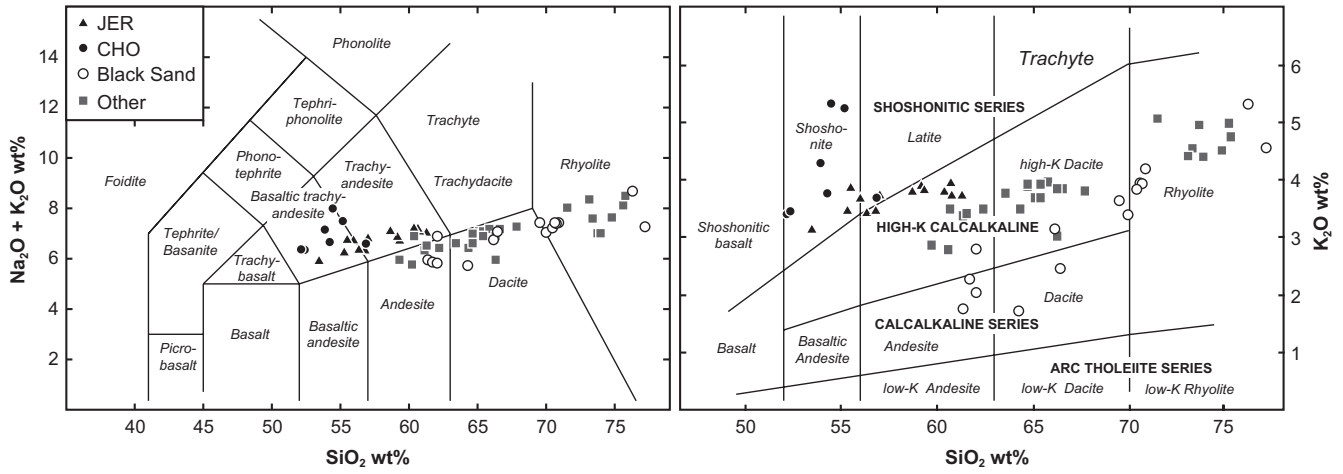

FIGURE 9 Diagrams of SiO_2 vs. $Na_2O + K_2O$ and SiO_2 vs. K_2O after Le Maitre et al. (2002) show areal bulk analyses by SEM-EDS of selected mafic grains handpicked from Quaternary Black Sand sample SA-261016-2 (white circles). Previously published data from the Pleistocene shoshonitic Jerónimo (JER) and Negro de Chorrillos (CHO) and various other Miocene volcanics are also plotted (Déruelle, 1991; Kay, Coira, Caffe, & Chen, 2010; Kay, Coira, & Viramonte, 1994; Petrinovic, Riller, Brod, Alvarado, & Arnosio, 2006; Schreiber & Schwab, 1991). The data show no correlation of the Quaternary Black Sand with any of the mafic lava flows, but have some similarities with known andesitic to rhyolitic ignimbrites and volcanics near the SAC area

deposits have a maximum depositional age of 1.1 Ma (Figure 8). Moreover, the zircon age spectra imply a source region that exposed largely 10.5 Ma and 4.5–4 Ma rocks, and to a lesser degree portions of Neoproterozoic-Cambrian and Palaeozoic basement rocks. The Late Miocene ages correspond well with the Tajamar ignimbrite sequence (10.3 Ma) associated with the Cerro Aguas Calientes caldera ca. 25 km to the west of the town of San Antonio (e.g. Petrinovic et al., 2010). To our knowledge there seems to be no local source for the Pliocene (4.5–4 Ma) zircons, suggesting that this age peak is caused by input from reworked ash-fall material, likely sourced in the Altiplano-Puna Volcanic Complex.

5.3 | Geochemistry

Major element compositions from SEM-EDS areal analysis of 12 volcanic lithic grains (fine grained to aphanitic and slightly porphyric) from SA-261016-2 (No. 2) of the Quaternary Black Sand indicate calcalkaline to high-K calcalkaline composition (Figure 9). They show no correlation with the Pleistocene mafic volcanic centres but rather indicate andesitic to rhyolitic sources. In addition to SiO_2 and total alkali concentrations, TiO_2 concentrations of <1.0 wt% and MgO of <3.0 wt% differ significantly from the mafic centres (Supporting information Table S6). The EDS small-scale areal analyses are supported by the petrography. Whereas the andesitic to dacitic volcanic grains contain phenocrysts of zoned orthopyroxene (Supporting information Figure S5b,e), plagioclase (An_{40-50}), and ±augite clinopyroxene, samples of rhyolitic composition contain quartz with resorption textures, plagioclase (An_{28-32}) and augite clinopyroxene (Supporting information Figure S5d). Some andesites show typical flow textures or vesicles (Supporting information Figure S5a,c). The rock composition may explain the dominant peak of 10.5 Ma in the detrital zircon age spectra of this deposit (Figure 8), which may imply that the major contribution of the material is sourced in at least one of the ubiquitous ignimbrite deposits of the same age (Petrinovic et al., 2010).

6 | DISCUSSION

In the following sections, we discuss the importance of aggradation and incision processes in the eastern part of the Puna Plateau in the light of different forcing mechanisms spanning from local to regional perspectives; in addition, we put our findings into the context of processes that drive the morphological and sedimentological evolution of orogenic plateaus in general.

6.1 | The Los Patos Conglomerate

The Los Patos Conglomerate (ca. 14.5 Ma) has recently been proposed to be related to a transient extensional basin associated with activity of the Calama–Olacapato-El Toro fault system (del Papa & Petrinovic, 2017). This conclusion is supported by the spatially limited extent of the conglomerate and the northerly transport directions of its constituents, the fining-upward trend, and its relatively short-lived depositional phase resembling the transition from an underfilled to an overfilled basin (del Papa & Petrinovic, 2017).

It is certainly not a coincidence that the Los Patos Conglomerate is confined to a relatively narrow, N-S-trending corridor, and the similarities to structurally confined

intermontane basins in the adjacent Eastern Cordillera are striking. For example, the width of the present-day exposure of the early-stage conglomerates in the neighbouring reverse-fault-bounded intermontane Humahuaca Basin (Tilcara Formation) or the Alfarcito Conglomerate in the Quebrada del Toro Basin is at most 3.5 km. Exposures of the Los Patos Conglomerate at the Corte Blanco section reveal an E-W extent of ca. 3 km – not considering a possible subsurface extent towards the west (Figure 6).

An alternative explanation of the Los Patos depositional setting may be analogous to the history of sedimentary records in the adjacent intermontane basins of Eastern Cordillera (e.g. Humahuaca, Toro, Angastaco). The sedimentary deposits of these basins reflect a record of initial basin-forming processes, associated with adjacent range uplift and enhanced conglomeratic sedimentation, accompanied by forcing of fluvial networks (Hain et al., 2011; Hilley & Strecker, 2005; Pingel, Strecker, Alonso, & Schmitt, 2013; Strecker et al., 2007). Other evidence supporting an intermontane basin evolution associated with the deposition of the Los Patos Conglomerate comes from the cooling/exhumation history of the adjacent mountain ranges. Multiple studies have documented that increased tectonic activity along the eastern Puna Plateau margin since ca. 20 Ma has led to the structural separation and loss of fluvial connectivity between the present-day plateau and the foreland. For example, uplift of the Luracatao Range in the Angastaco area at ca. 25.5°S lat, prevented eastward sediment transport by 20 Ma (Coutand et al., 2006; Deeken et al., 2006; Galli et al., 2014). Similarly, the Cachi Range, immediately to the northeast, experienced rapid exhumation and uplift by at least 15 Ma (Deeken et al., 2006; Pearson et al., 2012, 2013). Today, both of these ranges constitute the eastern margin of the Pastos Grandes Basin of the Puna at ca. 24.7°S lat; this area has been characterized by internal drainage conditions since ca. 12–10 Ma (Vandervoort, Jordan, Zeitler, & Alonso, 1995). Tectonic activity at that time is also documented from the Quebrada del Toro to the east of the SAC area. Here, the main basin-bounding Solá, Golgotá and San Bernardo faults are associated with syntectonic growth strata in their Mid-Miocene footwall deposits (Barres sandstone and Agujas conglomerate, DeCelles, Carrapa, Horton, & Gehrels, 2011; Mazzuoli et al., 2008; Pearson et al., 2013; Vezzoli, Acocella, Omarini, & Mazzuoli, 2012). Likewise, at 23.5°S lat, AFT-thermochronology suggests that the Sierra Alta, the western basin-bounding range of the Humahuaca Basin, underwent enhanced exhumation, and presumably surface uplift, between ca. 15 and 10 Ma (Deeken, Sobel, Haschke, & Riller, 2005); however, in this case, fluvial separation from the Puna Plateau may not have been established until ca. 4 Ma (Pingel et al., 2013).

At Corte Blanco, del Papa and Petrinovic (2017) report a fining-upward trend from a 15-m-thick section of the Los Patos Conglomerate. In the same area, Ramos (1973), however reported an at least 270-m-thick section with inverse grading. It is therefore possible that the more recent study may have missed a significant part of the section. An erosional unconformity between the $<14.5 \pm 0.5$ Ma Los Patos Conglomerate and the overlying 12.42 ± 0.04 Ma Viscachayoc Ignimbrite shows that conglomeratic deposition had already stopped by the time of the volcanic eruptions. Consequently, deposition may have lasted ca. 2.08 ± 0.50 Myr. However, since the base of the unit is not exposed (the onset of deposition may be older), the volcanic clasts dated near the base represent only a maximum depositional age (the sediment may be younger), and because the upper age constraint is a minimum age (i.e. the sediment is older than the ignimbrite), the actual time span of the depositional cycle remains uncertain. This also implies that it is not clear whether or not the conglomerate deposition was rather short lived as inferred earlier. Ultimately, we do not see strong support for the existence of a transient extensional basin setting and would like to propose an alternative depositional scenario to explain the Los Patos Conglomerate. We suggest that our model may be more in line with the general character of tectono-sedimentary evolution of other eastern Andean basins.

Accordingly, between <14.5 Ma and >12.4 Ma, the Los Patos Conglomerate was deposited on an erosional palaeotopography carved into the underlying, deformed Palaeocene units of the Salta Group (del Papa & Petrinovic, 2017). Outcrops of the Middle Eocene Casa Grande Formation (reviewed in Montero-López et al., 2016) near the eastern margin of the SAC area (along the Muñaño Fault) document a depositional environment in this region at least until the Middle Eocene and consequently imply a hiatus between both units of up to 23 Myr. This setting requires that the Early Miocene SAC area – similar to the neighbouring Pastos Grandes Basin in the south or the Salinas Grandes and Casa Grande basins in the north at that time – was still part of a fluvially connected and externally drained broken foreland system that did not promote deposition in isolated basin centres as observed today (Montero-López et al., 2016). On the contrary, this region of the Andes was eroding and sediments must have been routed towards the eastern foreland. Only during the onset of Miocene tectonism and surface uplift within the Eastern Cordillera (Coutand et al., 2006; Deeken et al., 2006; Pearson et al., 2012), sufficient topography must have been created to cause the deposition of coarse conglomerates such as the Los Patos Conglomerate. At least since then, sediment transport appears to have been diverted northward into the area of the present-day Salinas Grandes Basin and from there eastward towards the foreland, until the eastern Puna border was ultimately closed and fluvially severed by ca. 4 Ma (Pingel et al., 2013, 2014).

A similar observation was made for the Late Mio-Pliocene conglomerates and sandstones of the Maimará Formation in the Humahuaca Basin. These sediments also mark the onset

of renewed deposition in a tectonically active setting that transitioned from exhumation and basement erosion to deposition, once the landscape had gained pronounced relief and accommodation space to store incoming sediment (Pingel et al., 2013, 2014). The difference between both regions, however, is that in contrast to the Puna Plateau, the intermontane basins of the Eastern Cordillera were only transiently closed and never experienced the amount of orographic isolation that has typified the arid to hyper-arid environments of the Puna Plateau (Alonso, Gutiérrez, & Viramonte, 1984; Strecker et al., 2007, 2009).

6.2 | Mio-Pliocene tectono-sedimentary evolution

Following the structural and fluvial separation from the foreland and the deposition of the Los Patos Conglomerate, the SAC area experienced intense volcanic activity associated with extensive ignimbrite emplacement between 13 and 10 Ma, which included the Viscachayoc Ignimbrite (Petrinovic et al., 1999, 2010). A major unconformity at the top of this sequence marks a regional erosion event that preceded the following deposition of Mio-Pliocene fluvial sands and gravels of the SAC Formation. At the base, this formation is intercalated with two ash deposits of Late Miocene age: firstly, ca. 7.7–7.4 Ma white to grey volcanic ash and surge deposits, belonging to the ubiquitous, garnet-bearing Corte Blanco Tuff (Toba I, Viramonte et al., 1994); and secondly, a tuff with a maximum depositional age of ca. 6.4 Ma (this study). Two prominent, sub-horizontal volcanic ashes higher up in the section and ca. 40 m below the terrace surface, east of the town of San Antonio (No. 4, Figure 3), are 5.7 and 5.6 Ma.

The Corte Blanco section (Figures 3 and 6) provides unique insights into the deformation and depositional history of the northeastern Puna margin. Here, the Los Patos River has cut through most of the regionally distributed sedimentary units, ranging from Quaternary gravels at the top, to the Palaeocene-Eocene sections of the upper Salta Group below. The main structure at this site is a NNE-SSW-striking, asymmetric, west-vergent anticline with decreasing western limbs (70–0°W) in the lower sections of the Mio-Pliocene SAC Formation, which documents syntectonic growth since at least 7.7–7.4 Ma. Farther away from this structure to the west, most of the outcrops of the SAC Formation record sub-horizontal bedding. Exceptions to the generally undeformed state of the SAC Formation are found west of San Antonio where the SAC Formation unconformably overlies Puncoviscana basement rocks. Here, the Mio-Pliocene sediments are often deformed forming open, low-amplitude folds. Some isolated outcrops along the Sierra de los Cobres show more clear evidence for Mio-Pliocene basement-involved deformation. However, this deformation pattern is only locally found and most likely related to more complex basement deformation in the area. Fold axes associated with this deformation trend WNW to NW, inferred to have been associated with structures along the Calama–Olacapato–El Toro lineament (Acocella et al., 2011).

Most of the SAC strata are covered by an up to 20-m-thick succession of Quaternary cobble to boulder conglomerates from proximal, southerly sources, intercalated with the Quaternary Black Sand (≤1.1 Ma); subsequently, the SAC area was incised.

6.3 | Depositional age and origin of the Quaternary Black Sand

The Quaternary Black Sand is a prominent marker bed in the uppermost sectors of the stratigraphic sequence in the SAC area (Figure 7; Supporting information Figure S2). However, unlike Seggiaro et al. (2016) we consider this deposit not to be a product of the shoshonitic Negro de Chorrillos volcanic eruption ca. 0.2 Myr ago. Instead, our regional observations and analytical data indicate that the Quaternary Black Sand is the erosional product of mainly andesitic, dacitic and rhyolitic source rocks; in addition, its deposition took place prior to the Chorrillos eruption. Most relevant for this assessment is (a) the major element geochemistry of handpicked mafic grains from sample SA-261016-2 near the town of San Antonio (Figure 2, No. 3) that show no relation to any of the local mafic volcanic centres (Figure 9). Hence, the lithic components that constitute this deposit cannot have originated from the high-K calc-alkaline and shoshonitic products of Pleistocene mafic volcanic centres in the SAC area. (b) Detrital zircon ages from two sand samples – one collected 4 km NNW of the Negro de Chorrillos volcano (No. 1) and the other near the top of the terrace surface next to the town of San Antonio (No. 2) – reveal very similar age spectra that imply a mixed source with major contribution from 4 to 4.5 Ma and 10.5 Ma rocks and a minor contribution from Cambrian and Precambrian lithologies. The youngest zircon dated is 1.1 Ma, which we interpret as the maximum depositional age for the Quaternary Black Sand. (c) All investigated outcrops that involve Quaternary Black Sand have a strong affiliation with sub-rounded to rounded cobble to boulder conglomerates and other fluvial/alluvial gravel. Even on a meso- to microscopic scale, most components of the sands are at least sub-rounded, suggesting transport mechanisms other than air-fall and/or pyroclastic surging (Supporting information Figure S3). (d) Finally, other localities, such as outcrop No. 2, which is an integral part of the terrace system of the SAC area and whose deposits are also interbedded with cobble to boulder conglomerates ca. 80 m above the San Antonio River, show that the Chorrillos volcano could not have produced the Quaternary Black Sand. Although the observed course of the Chorrillos lava flow indicates an already dissected landscape, exposures of the Quaternary Black Sand

are only found at levels associated with the pre-incised palaeotopography of the SAC area (Figure 10).

In summary, the spatial distribution and stratigraphic position of the Quaternary Black Sand above the present-day baselevel, the inferred fluvial transport mechanism and the common occurrence of the Quaternary Black Sand together with fluvial/alluvial conglomerates and gravel, suggests that their deposition took place during a time and in a basin setting in which the elevated palaeosurface of the SAC area was a contiguous feature that was largely still intact and active as a transport surface.

6.4 | Mid-Pleistocene river incision

6.4.1 | Timing of river incision

To assess the surface processes and rates that shaped the SAC area during the Pleistocene, it is important to constrain the timing of the river incision. Unfortunately, there are currently no absolute age determinations available for the terrace surfaces. However, we can indirectly determine the timing of the incision. Firstly, the distribution of Quaternary deposits suggests that the Black Sand and the Quaternary conglomerates belong to a formerly contiguous transport and depositional surface. These units are always found near or above the elevation of the reconstructed palaeosurface (Figure 10). Detrital zircons obtained in these units suggest a maximum depositional age of ca. 1.1 Ma. Secondly, stratigraphic relationships between the Quaternary conglomerates and gravels and the 0.78-Myr-old San Jerónimo lava flow help to further refine the age of the depositional surface. Locally, the Quaternary Black Sand onlap the lava (Supporting information Figure S2), which requires that the palaeosurface was intact when the San Jerónimo flow was emplaced. Importantly, by 0.2 Ma a second lava flow sourced from the Negro de Chorrillos volcano, utilized an incised valley, which was adjusted to a baselevel similar to the modern trunk stream (Figure 10). In summary, when the Jerónimo volcano erupted 0.78 Myr ago, the SAC area and its elevated palaeosurface were largely intact, and incision must have been completed prior to 0.2 Ma.

6.4.2 | Excavation rate

Assuming that the areal incision is the result of continuous landscape denudation, a mean catchment-wide erosion rate can be estimated for the SAC region. To excavate the calculated sediment volume of 6.5 ± 2.0 km^3 from the SAC catchment (1,463 km^2) over the course of 0.58 Myr, the basin-wide excavation rate must have been on the order of 0.01 mm/year. This rate is compatible with modern catchment-wide erosion rates of 0.02 mm/year or less (Bookhagen & Strecker, 2012); both rates highlight reduced surface-process rates in the internally drained Puna Plateau. Moreover, if this relationship is compared to other incised sedimentary basins and sub-catchments in NW Argentina, there appears to be a first-order correlation, which suggests that excavation rates may represent reasonable indicators of surface-process rates in alluvial river settings. For example, we estimate the excavation rate of the Casa Grande Basin (CGB: 767 km^2, Figure 1) to the northeast of our study area using the chronostratigraphy of Streit et al. (2015) and a calculated volume of removed sediment of 6.8 km^3 (Supporting information Figure S6). There, an 800 ka tuff in the CGB's topmost basin strata suggests renewed connectivity and subsequent excavation of the basin sediments, resulting in a minimum excavation rate of ca. 0.01 mm/year. Catchment-wide denudation rates are only reported from the larger Río Yacoraite catchment, sampled

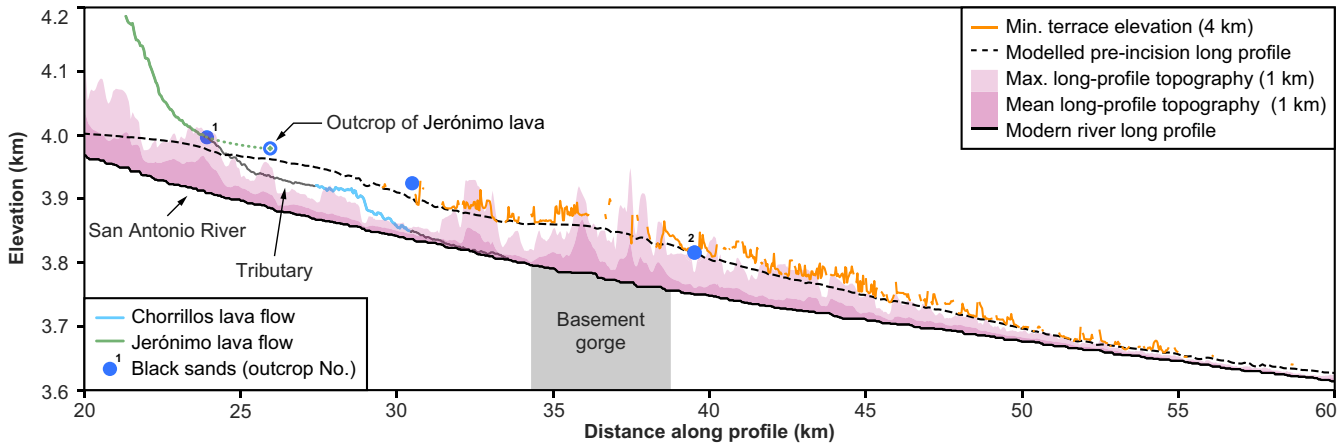

FIGURE 10 Longitudinal river profiles (from SRTM 30 m) of the lower reach of the San Antonio River and a minor tributary in the west of San Antonio town (dashed river section in Figure 3). Along this minor tributary, the position of two different basalt flows is plotted highlighting their spatiotemporal separation. Although outcrops of the 0.78 Ma Jerónimo flow are limited to above the reconstructed palaeotopography (dashed line), the 0.2 Ma Chorrillos flow appears to have been emplaced in the presently incised landscape. Blue circles represent outcrops of Quaternary Black Sand projected along the profile. Their continuous position above the terrace surface documents a deposition before the incision took place

20 km east of the CGB outlet, and yield 0.03–0.04 mm/year (Bookhagen & Strecker, 2012; Schildgen et al., 2016). Another sub-basin in the southern Humahuaca Basin, the Tumbaya area (145 km^2), was excavated after 75.5 ± 1.3 ka (^{10}Be, Schildgen et al., 2016). The estimated sediment volumes removed amount to 0.8 km^3, resulting in a minimum excavation rate of 0.08 mm/year (Supporting information Figure S7). Catchment-wide denudation rates from cosmogenic ^{10}Be concentrations of modern river sands yielded ca. 0.08 mm/year (Schildgen et al., 2016).

6.4.3 | Causes of river incision

Baselevel change

Comparing the longitudinal river profiles of the reconstructed palaeo-landscape with the profile of the modern San Antonio River shows that the slopes of both profiles converge towards the northern outlet of the SAC area. Not only does this geometry show that the regional baselevel was at the same level before and after the incision, but also that the average palaeo-landscape of the SAC area must have been steeper compared to today. This conclusion is supported by decreasing steepness indices between the downstream projection of the uppermost, un-dissected reach of the San Antonio River ($k_s = 92$) and the lower reach of the modern river profile ($k_s = 75$; Figure 4). In this context it is interesting that <4.2 Ma sediments in the neighbouring Humahuaca Basin do not record Puna-derived clasts, which suggests that the tectonically controlled watershed between the Puna Plateau and the externally drained Eastern Cordillera (Sierra Alta) had been established by that time (Pingel et al., 2013, 2014). With the exception of variable fluvial connectivity between the Casa Grande Basin (a sub-basin of the Puna) and the Humahuaca Basin (Jirón, 2015; Streit et al., 2015), there appears to have been no further connectivity of the internally and externally drained regions of the Andes in NW Argentina. This implies that the Salinas Grandes Basin has been the regional depositional centre and ultimate baselevel since at least the Pliocene.

Tectonics

Although, strata underlying the Mio-Pliocene SAC Formation are usually strongly deformed, this unit itself only exhibits local deformation along the western basin margin and growth strata in the central part of the SAC area at the Corte Blanco site (Figures 3 and 6). The upper, Pliocene sections of the SAC Formation and the overlying Quaternary units generally appear to be undeformed. To date, there is only one documented site of deformed Quaternary Black Sand revealing open folding and minor thrust faulting at outcrop No. 1 (Seggiaro et al., 2016). Another locality discussed by these authors, shows strike-slip and thrust faulting in supposedly Quaternary strata near Corte Blanco. Our observations, however, suggest that these strata are part of the upper SAC formation, and thus Late Mio-Pliocene in age.

Deep earthquakes below 150 km associated with the subducting Nazca plate are very common in the study area and the neighbouring regions, but shallow crustal earthquakes are very rare, rendering this part of the Puna Plateau essentially aseismic (ANSS Comprehensive Earthquake Catalog); the absence of seismic events with ground-rupturing magnitudes is in line with the lack of pronounced deformation phenomena in Quaternary strata in this part of the Puna.

Normalized steepness values (k_{sn}) of the main river segments in the SAC region display no major knickzones, except for areas in the SW and S where the k_{sn} in part exceeds values of 450 (Supporting information Figure S4). These areas are underlain by basement rocks of the Faja Eruptiva (Ordovician) and Puncoviscana (Precambrian) formations, suggesting a lithological rather than a tectonic control of the river steepness. Finally, there is no prominent structure crossing the San Antonio River and its tributaries that would enable catchment-wide uplift; where the river crosses structural discontinuities there are no knickpoints that would indicate tectonic activity.

Climate

The inferred readjustment of the fluvial network (i.e. incision and reduced channel gradients) together with the unlikely case of a baselevel change in this setting is most likely a response to climatic forcing (Norton & Schlunegger, 2018; Schlunegger, Norton, & Zeilinger, 2011). This may have been associated with a relative increase in river discharge, either due to increased or more variable rainfall conditions or reduced sediment supply into the river network. The latter seems, however, implausible, because large portions of the hillslopes of the SAC area are composed of easily erodible Mio-Pliocene volcanic units.

After 0.8 Ma, the Casa Grande Basin in the north was reconnected with the Humahuaca Basin and ca. 7 km^3 of sediments were removed from the basin (Streit et al., 2015). Within a similar time frame, between about 1.0 and 0.8 Ma, large volumes of conglomerates were accumulated in the intermontane basins of the eastern Cordillera, that is, the Humahuaca Basin (Strecker et al., 2007; Pingel et al., 2013), the Quebrada del Toro Basin (Marrett & Strecker, 2000; Strecker et al., 2007) and in the Calchaquí valley (Pingel et al., 2016). In at least two of these basins (i.e. Humahuaca and Toro basins), the aggradation of conglomerates marks the onset of possibly climate-driven basin fill and excavation cycles in this part of the Andes (Hilley & Strecker, 2005; Pingel et al., 2013; Schildgen et al., 2016; Tofelde et al., 2017).

We hypothesize that the similar timing of incision on the eastern Puna Plateau (SAC and CGB) and the onset of oscillatory basin fill and excavation cycles in the adjacent intermontane basins of the Eastern Cordillera after 800 ka have a mutual climatic control, possibly associated with the intensification of global glacial-interglacial cycles following

the Mid-Pleistocene Climate Transition (ca. 950–850 ka, Mudelsee & Schulz, 1997). This transition was not only characterized by a shift in sea-surface temperature oscillations from 41 to 100 kyr cycles – the dominant cycle recognized in the Pleistocene terrace sequences in the Toro Basin (Tofelde et al., 2017) – but also by major changes in the duration and intensity of glacial cycles (Berger, Li, & Loutre, 1999). It has been suggested that during glacial periods, the Intertropical Convergence Zone (ITCZ) over South America had shifted far southward (Broccoli, Dahl, & Stouffer, 2006) leading to enhanced moisture transport via the South-American low-level jet and increased moisture availability in the highlands of NW Argentina (Haselton, Hilley, & Strecker, 2002; Vizy & Cook, 2007). However, the interior of the orogen was not affected by this increase in the same way as the orogenic flanks, as is shown by areally much more limited, and a westward-decreasing impact of Pleistocene glaciations in the Puna Plateau (Haselton et al., 2002; Luna et al., 2018). This is compatible with the notion of existing effective orographic barriers along the eastern Andean plateau area: The existence of these barriers and resulting diversions of atmospheric flow patterns results in decreased moisture availability towards the orogen interior. Such a non-uniform impact of global/regional climate change could explain the variable effects on surface processes and landscape evolution across the eastern Andean flanks since at least the Middle Pleistocene.

6.5 | Regional implications for plateau building and deformation processes

The SAC area provides a unique window through which to observe the potential interplay between tectonics, climate-driven surface processes and the long-term evolution of topography and relief in an orogenic plateau – that is, in this case, a plateau that has been largely maintained as a geomorphic entity. Here, the different forcing mechanisms on plateau morphology can be evaluated in a currently arid and internally drained setting that has alternated between episodes of aridity and increased moisture availability and run-off, thereby modifying sediment production, transport and deposition. Importantly, these oscillations also affected the intermontane sedimentary basins along the eastern flanks of the plateau, where the combined effects of tectonic uplift, deformation and superposed climate change resulted in more frequent, but relatively thin sedimentary fills during limited drainage conditions (Pingel et al., 2013; Schildgen et al., 2016; Strecker et al., 2007; Tchilinguirian & Pereyra, 2001; Tofelde et al., 2017). These episodes were followed by re-establishment of fluvial connectivity with the foreland, down-cutting and sediment removal from the orogen, which generated large peak-to-basin relief ratios in the intermontane basins (Figure 2) (Hilley & Strecker, 2005; Strecker et al., 2009). In contrast, the compressional basin-and-range topography of the Puna has developed into an environment of decreased internal relief due to maintained internal drainage conditions, erosion of the intervening high-relief mountain ranges and continued sediment storage.

The Puna basins primarily receive sediments from the erosion of surrounding ranges, evaporative mineral precipitation in transient lacustrine environments and protracted volcanic activity (Alonso, Jordan, Tabbutt, & Vandervoort, 1991; Petrinovic et al., 1999). These filling processes occur simultaneously, but the nature of infill is determined by locally prevailing climatic conditions and the scale of volcanism on the Puna. Following the initial basin formation, in the northern sectors of the present-day Puna Plateau, tectonism has influenced basin-scale sedimentation processes only to a minor degree and activity of range-bounding faults has been negligible during the Late Miocene and Pleistocene (Coutand et al., 2001; Gangui, 1998; Gubbels, Isacks, & Farrar, 1993). This seems surprising at first since the plateau is located along a convergent plate boundary and structures with protracted shortening would be expected. However, it has been suggested that when large amounts of sediment are trapped in a fault-bounded basin, deformation may be driven to exterior regions of the orogen as a result of increased lithostatic stresses and locking of basin-bounding fault structures (García-Castellanos, 2007; Sobel et al., 2003; Strecker et al., 2007). Increased loading at the onset of internal drainage and redistribution of mass within the orogen, therefore, provide a causal link between the efficiency of erosion, the existence of an internally drained plateau and the concentration of deformation along its margin.

Indeed, such links between muted fault activity and sedimentary fill/loading, and vice versa, the reactivation of faults associated with basin incision and unloading have been demonstrated in numerical experiments (Ballato, Brune, & Strecker, 2019) and were proposed for the Plio-Pleistocene history of virtually all intermontane basins east of Puna Plateau (Hilley & Strecker, 2005; Pingel et al., 2013; Strecker et al., 2007, 2009). This emphasizes the importance of orographically induced aridity on maintaining internally drained orogenic plateaus that would otherwise experience changes in the near-surface stress field through basin excavation and renewed plateau-wide contractional tectonism. Instead, the high-elevation basins in the eastern sector of the Puna, with their thick fills and low-relief characteristics, appear to be the areas of sustained stability.

Similar to other Cenozoic plateaus, the observations from the eastern Puna Plateau confirm the notion that lateral plateau growth is accomplished via (a) initial crustal compartmentalization and formation of elevated intermontane basins as a result of progressively outward migrating deformation and range uplift; (b) orographically induced aridification; (c) development of restricted to closed-drainage conditions; (d) and finally internal relief reduction by bedrock erosion and

basin filling to potentially form large coalesced basins as observed today (Allen et al., 2013; García-Castellanos, 2007; Liu-Zeng et al., 2008; Sobel et al., 2003; Strecker et al., 2007). As such, these basins and the relief-reducing processes acting upon the plateau environments are quite similar to those that have been proposed to drive the morphologic and sedimentary evolution of basins on the Tibetan Plateau (Liu-Zeng et al., 2008; Métivier et al., 1998).

7 | CONCLUSIONS

In this study, we investigated the tectono-sedimentary evolution of the San Antonio de los Cobres area; a sub-catchment of the internally drained Salinas Grandes Basin located at the eastern Andean Puna Plateau margin. By comparing the characteristics of depositional regimes, associated with tectonic range uplift and intermontane basin formation across the eastern Andes, we suggest that the Late Miocene onset of conglomerate deposition in the SAC area is related to similar orogenic processes. The Los Patos Conglomerate of the San Antonio area may thus represent initial clastic accumulation related to the topographic growth of the present-day eastern Puna Plateau border.

Using U-Pb zircon geochronology, we refined the Miocene to Pleistocene stratigraphy of the San Antonio de los Cobres area. Deposits previously grouped as Pleistocene-Holocene tuff-bearing and terrace-forming fanglomerates, can now clearly be separated into distinct stratigraphic units; these are the Late Mio-Pliocene San Antonio de los Cobres Formation (*nomen novum*, ca. >7.4–<5 Ma) and Quaternary cobble to boulder conglomerates (>1.1–ca. 0.8 Ma). These conglomerates formed a broad area of aggradation that later became dissected, with sediment being transferred within the Puna.

Landscape reconstruction and additional sedimentary and geochemical provenance indicators helped to decipher the processes that led to the evacuation of $6.5 \pm 2.0\ km^3$ of basin filling material northward into the Salinas Grandes Basin since at least 0.78 Ma. The timing for this incision and other coeval sedimentary processes in the adjacent Eastern Cordillera suggest a regional climate change. We speculate that this climate change was caused by the onset of more efficient glacial-interglacial cycles following the Mid-Pleistocene Climate Transition, which increased moisture supply into the orogen interior, thereby enhancing fluvial run-off and incision.

Finally, we explored the importance of crustal deformation, topographic build-up and ensuing (orographically induced) aridification and reduced surface processes in creating and maintaining internally drained orogenic plateau regions. We conclude that, although plateaus are among the largest geomorphic features on Earth, their formation may be the result of a delicate interplay between uplift along the orogenic front and a number of orographic effects that modify rainfall amount, run-off, erosion and sediment transport/distribution in the hinterland.

ACKNOWLEDGMENTS

This research was funded by Deutsche Forschungsgemeinschaft (DFG) grants STR373/21-1 and STR373/16-1 to M. Strecker. Additional support came from DFG grant STR 373/34-1 and the Brandenburg Ministry of Sciences, Research and Cultural Affairs, Germany, within the framework of the international research training group IGK2018 SuRfAce processes, TEctonics and Georesources: The Andean foreland basin of Argentina (StRATEGy). We thank A. Rosner and M. Lang (Potsdam) for field assistance and V. Ramos, A. Rohrmann and S. Tofelde for prolific discussions. We are also grateful for detailed and constructive reviews by Burch Fisher, Alan Carroll and an anonymous reviewer.

REFERENCES

Acocella, V., Gioncada, A., Omarini, R., Riller, U., Mazzuoli, R., & Vezzoli, L. (2011). Tectono-magmatic characteristics of the Calama-Olacapato-El Toro Fault Zone (Puna and Eastern Cordillera), Central Andes. *Tectonics*, *30*, 1–19. http://doi.org/10.1029/2010TC002854

Allen, M. B., Saville, C., Blanc, E. J.-P., Talebian, M., & Nissen, E. (2013). Orogenic plateau growth: Expansion of the Turkish-Iranian Plateau across the Zagros fold-and-thrust belt. *Tectonics*, *32*(2), 171–190. https://doi.org/10.1002/tect.20025

Alonso, R. N., Bookhagen, B., Carrapa, B., Coutand, I., Haschke, M., Hilley, G. E., … Villanueva, A. (2006). Tectonics, climate, and landscape evolution of the southern Central Andes: The Argentine Puna Plateau and adjacent regions between 22 and 30°S. In O. Oncken, G. Chong, G. Franz, P. Giese, H.-J. Götze, V. A. Ramos, et al. (Eds.), *The Andes* (pp. 265–283). Berlin Heidelberg: Springer. https://doi.org/10.1007/978-3-540-48684-8_12

Alonso, R. N., Gutiérrez, R., & Viramonte, J. (1984). Megacuerpos salinos cenozoicos de la Puna Argentina(Vol. 1, pp. 25–42). Presented at the IX Congreso Geológico Argentino, IX Congreso Geológico Argentino.

Alonso, R. N., Jordan, T. E., Tabbutt, K. T., & Vandervoort, D. S. (1991). Giant evaporite belts of the Neogene central Andes. *Geology*, *19*(4), 401–404. https://doi.org/10.1130/0091-7613(1991)019<0401:GEBOTN>2.3.CO;2

Andriessen, P. A. M., & Reutter, K. J. (1994). K-Ar and Fission Track Mineral Age Determination of Igneous Rocks Related to Multiple Magmatic Arc Systems Along the 23°S Latitude of Chile and NW Argentina. In K.-J. Reutter, E. Scheuber, & P. J. Wigger (Eds.), *Tectonics of the Southern Central Andes* (pp. 141–153). Berlin Heidelberg: Springer. https://doi.org/10.1007/978-3-642-77353-2_10

Aquater. (1980). *Exploración Geotérmica del cerro Tuzgle, provincia de Jujuy, República Argentina* (pp. 1–115). Buenos Aires, Argentina: Secretaría de Energía de la Nación.

Ballato, P., Brune, S., & Strecker, M. R. (2019). Sedimentary loading–unloading cycles and faulting in intermontane basins: Insights from

numerical modeling and field observations in the NW Argentine Andes. *Earth and Planetary Science Letters*, *506*, 388–396.

Ballato, P., Stockli, D. F., Ghassemi, M. R., Landgraf, A., Strecker, M. R., Hassanzadeh, J., … Tabatabaei, S. H. (2013). Accommodation of transpressional strain in the Arabia-Eurasia collision zone: New constraints from (U-Th)/He thermochronology in the Alborz mountains, north Iran. *Tectonics*, *32*(1), 1–18. https://doi.org/10.1029/2012TC003159

Berger, A., Li, X. S., & Loutre, M. F. (1999). Modelling northern hemisphere ice volume over the last 3 Ma. *Quaternary Science Reviews*, *18*(1), 1–11.

Bianchi, A. R., & Yañez, C. E. (1992). *Las precipitaciones en el Noroeste Argentino*, 2nd ed. Salta, Argentina: Instituto Nacional de Tecnologia Agropecuaria, Estacíon Experimental Agropecuaria Salta.

Blasco, G., & Zappettini, E. (1996). Hoja geológica San Antonio de los Cobres. 2566-1, Programa Nacional de Cartas Geológicas 1:250.000(Vol. 217). Servicio Geológico Minero Argentino.

Bookhagen, B., & Burbank, D. W. (2006). Topography, relief, and TRMM-derived rainfall variations along the Himalaya. *Geophysical Research Letters*, *33*(8), 1–5. https://doi.org/10.1029/2006GL026037

Bookhagen, B., & Strecker, M. R. (2008). Orographic barriers, high-resolution TRMM rainfall, and relief variations along the eastern Andes. *Geophysical Research Letters*, *35*, L06403. https://doi.org/10.1029/2007GL032011

Bookhagen, B., & Strecker, M. R. (2012). Spatiotemporal trends in erosion rates across a pronounced rainfall gradient: Examples from the southern Central Andes. *Earth and Planetary Science Letters*, *327–328*, 97–110. https://doi.org/10.1016/j.epsl.2012.02.005

Broccoli, A. J., Dahl, K. A., & Stouffer, R. J. (2006). Response of the ITCZ to Northern Hemisphere cooling. *Geophysical Research Letters*, *33*(1), 1–4. https://doi.org/10.1029/2005GL024546

Carroll, A. R., Graham, S. A., & Smith, M. E. (2010). Walled sedimentary basins of China. *Basin Research*, *22*(1), 17–32. https://doi.org/10.1111/j.1365-2117.2009.00458.x

Coutand, I., Carrapa, B., Deeken, A., Schmitt, A. K., Sobel, E. R., & Strecker, M. R. (2006). Propagation of orographic barriers along an active range front: Insights from sandstone petrography and detrital apatite fission-track thermochronology in the intramontane Angastaco basin, NW Argentina. *Basin Research*, *18*(1), 1–26. https://doi.org/10.1111/j.1365-2117.2006.00283.x

Coutand, I., Cobbold, P. R., de Urreiztieta, M., Gautier, P., Chauvin, A., Gapais, D., … López-Gamundí, O. (2001). Style and history of Andean deformation, Puna plateau, northwestern Argentina. *Tectonics*, *20*(2), 210–234. https://doi.org/10.1029/2000TC900031

DeCelles, P. G., Carrapa, B., Horton, B. K., & Gehrels, G. E. (2011). Cenozoic foreland basin system in the central Andes of northwestern Argentina: Implications for Andean geodynamics and modes of deformation. *Tectonics*, *30*(TC6013), TC6013. https://doi.org/10.1029/2011TC002948

Deeken, A., Sobel, E. R., Coutand, I., Haschke, M., Riller, U., & Strecker, M. R. (2006). Development of the southern Eastern Cordillera, NW Argentina, constrained by apatite fission track thermochronology: From early Cretaceous extension to middle Miocene shortening. *Tectonics*, *25*, 1–21. https://doi.org/10.1029/2005TC001894

Deeken, A., Sobel, E. R., Haschke, M., & Riller, U. (2005). Age of initiation and growth pattern of the Puna plateau, NW-Argentina, constrained by AFT thermochronology. *19th Colloquium on Latin American Geosciences, Abstract Volume Terra Nostra*, *5*(1), 39.

Déruelle, B. (1991). Petrology of Quaternary shoshonitic lavas of northwestern Argentina. *Geological Society of America Special Papers*, *265*, 201–216.

Fielding, E., Isacks, B. L., Barazangi, M., & Duncan, C. (1994). How flat is Tibet? *Geology*, *22*(2), 163.

Flint, J. J. (1974). Stream gradient as a function of order, magnitude, and discharge. *Water Resources Research*, *10*(5), 969–973. https://doi.org/10.1029/WR010i005p00969

Galli, C. I., Coira, B., Alonso, R. N., Reynolds, J. H., Matteini, M., & Hauser, N. (2014). Tectonic controls on the evolution of the Andean Cenozoic foreland basin: Evidence from fluvial system variations in the Payogastilla Group, in the Calchaquí, Tonco and Amblayo Valleys, NW Argentina. *Journal of South American Earth Sciences*, *52*(C), 234–259. https://doi.org/10.1016/j.jsames.2014.03.003

Gangui, A. H. (1998). *A combined Structural Interpretation based on Seismic Data and 3-D Gravity Modeling in the Northern Puna/Eastern Cordillera, Argentina*, 1st ed., Vol. Reihe B. Berlin, Germany: Selbstverlag Fachbereich Geowissenschaften, FU Berlin.

García-Castellanos, D. (2007). The role of climate during high plateau formation. Insights from numerical experiments. *Earth and Planetary Science Letters*, *257*(3–4), 372–390. https://doi.org/10.1016/j.epsl.2007.02.039

Gubbels, T. L., Isacks, B. L., & Farrar, E. (1993). High-level surfaces, plateau uplift, and foreland development, Bolivian central Andes. *Geology*, *21*, 695–698.

Hain, M. P., Strecker, M. R., Bookhagen, B., Alonso, R. N., Pingel, H., & Schmitt, A. K. (2011). Neogene to Quaternary broken foreland formation and sedimentation dynamics in the Andes of NW Argentina (25 S). *Tectonics*, *30*, 1–27. https://doi.org/10.1029/2010TC002703

Haselton, K., Hilley, G., & Strecker, M. R. (2002). Average Pleistocene climatic patterns in the southern Central Andes: Controls on mountain glaciation and paleoclimate implications. *The Journal of Geology*, *110*(2), 211–226.

Heidarzadeh, G., Ballato, P., Hassanzadeh, J., Ghassemi, M. R., & Strecker, M. R. (2017). Lake overspill and onset of fluvial incision in the Iranian Plateau: Insights from the Mianeh Basin. *Earth and Planetary Science Letters*, *469*, 135–147. https://doi.org/10.1016/j.epsl.2017.04.019

Hilley, G. E., & Strecker, M. R. (2005). Processes of oscillatory basin filling and excavation in a tectonically active orogen: Quebrada del Toro Basin, NW Argentina. *Geological Society of America Bulletin*, *117*(7–8), 887–901. https://doi.org/10.1130/1325602.1

Hongn, F. D., del Papa, C. E., Powell, J., Petrinovic, I., Mon, R., & Deraco, V. (2007). Middle Eocene deformation and sedimentation in the Puna-Eastern Cordillera transition (23–26 S): Control by preexisting heterogeneities on the pattern of initial Andean shortening. *Geology*, *35*(3), 271–274. https://doi.org/10.1130/G23189A.1

Jirón, R. L. (2015). *Interactions of tectonics, climate, and deposition in intermontane basins on the margin of the Puna Plateau, NW Argentina*. Santa Barbara, CA: University of California Santa Barbara.

Jordan, T. E., & Alonso, R. N. (1987). Cenozoic Stratigraphy and Basin Tectonics of the Andes Mountains, 20–28 South Latitude. *AAPG Bulletin*, *71*(1), 49–64. https://doi.org/10.1306/94886D44-1704-11D7-8645000102C1865D

Kay, S. M., Coira, B. L., Caffe, P. J., & Chen, C.-H. (2010). Regional chemical diversity, crustal and mantle sources and evolution of central Andean Puna plateau ignimbrites. *Journal of Volcanology and*

Geothermal Research, *198*(1–2), 81–111. https://doi.org/10.1016/j.jvolgeores.2010.08.013

Kay, S. M., Coira, B., & Viramonte, J. (1994). Young mafic back arc volcanic rocks as indicators of continental lithospheric delamination beneath the Argentine Puna Plateau, central Andes. *Journal of Geophysical Research*, *99*(B12), 24323–24339. https://doi.org/10.1029/94JB00896

Kirby, E., & Whipple, K. (2001). Quantifying differential rock-uplift rates via stream profile analysis. *Geology*, *29*(5), 415–418. https://doi.org/10.1130/0091-7613(2001) 029<0415:QDRURV>2.0.CO;2

Kirby, E., & Whipple, K. X. (2012). Expression of active tectonics in erosional landscapes. *Journal of Structural Geology*, *44*, 54–75. https://doi.org/10.1016/j.jsg.2012.07.009

Le Maitre, R. W., Streckeisen, A., Zanettin, B., Le Bas, M. J., Bonin, B., & Bateman, P. (Eds.) (2002). *Igneous Rocks: A Classification and Glossary of Terms edited by R. W. Le Maitre*. Cambridge, UK: Cambridge University Press. https://doi.org/10.1017/CBO9780511535581

Letcher, A. J. (2007). *Deformation history of the Susques basin (˜23°S, 66°W), Puna Plateau, NW Argentina: New constraints by apatite (U-Th)/He thermochronology and 40Ar/39Ar geochronology, and implications for plateau formation in the central Andes*. MSc Thesis. Stanford, California: Stanford University.

Liu-Zeng, J., Tapponnier, P., Gaudemer, Y., & Ding, L. (2008). Quantifying landscape differences across the Tibetan plateau: Implications for topographic relief evolution. *Journal of Geophysical Research*, *113*, F04018. https://doi.org/10.1029/2007JF000897

Luna, L. V., Bookhagen, B., Niedermann, S., Rugel, G., Scharf, A., & Merchel, S. (2018). Glacial chronology and production rate cross-calibration of five cosmogenic nuclide and mineral systems from the southern Central Andean Plateau. *Earth and Planetary Science Letters*, *500*, 242–253. https://doi.org/10.1016/j.epsl.2018.07.034

Marquillas, R. A., del Papa, C. E., & Sabino, I. F. (2005). Sedimentary aspects and paleoenvironmental evolution of a rift basin: Salta Group (Cretaceous-Paleogene), northwestern Argentina. *International Journal of Earth Sciences (Geol. Rundschau)*, *94*(1), 94–113. https://doi.org/10.1007/s00531-004-0443-2

Marrett, R. A., & Strecker, M. R. (2000). Response of intracontinental deformation in the central Andes to late Cenozoic reorganization of South American Plate motions. *Tectonics*, *19*(3), 452–467. https://doi.org/10.1029/1999TC001102

Masek, J., Isacks, B. L., Gubbels, T. L., & Fielding, E. (1994). Erosion and tectonics at the margins of continental plateaus. *Journal of Geophysical Research*, *99*(B7), 13941–13956.

Mazzuoli, R., Vezzoli, L., Omarini, R., Acocella, V., Gioncada, A., Matteini, M., … Scaillet, S. (2008). Miocene magmatism and tectonics of the easternmost sector of the Calama–Olacapato–El Toro fault system in Central Andes at ~24 S: Insights into the evolution of the Eastern Cordillera. *Geological Society of America Bulletin*, *120*(11–12), 1493–1517. https://doi.org/10.1130/B26109.1

Mendez, V., Navarini, A., Plaza, D., & Viera, V. (1973). Faja Eruptiva de la Puna Oriental. *Actas Del 5th Congreso Geológico Argentino*, *4*, 89–100. https://doi.org/10.1029/2000TC900031/full

Métivier, F., Gaudemer, Y., Tapponnier, P., & Meyer, B. (1998). Northeastward growth of the Tibet plateau deduced from balanced reconstruction of two depositional areas. *The Qaidam and Hexi Corridor basins, China*, *17*(6), 823–842. http://doi.org/10.1029/98TC02764

Montero-López, C., del Papa, C. E., Hongn, F. D., Strecker, M. R., & Aramayo, A. (2016). Synsedimentary broken-foreland tectonics during the Paleogene in the Andes of NW Argentine: New evidence from regional to centimetre-scale deformation features. *Basin Research*, *30*(1), 1–18. https://doi.org/10.1111/bre.12212

Mudelsee, M., & Schulz, M. (1997). The Mid-Pleistocene climate transition: Onset of 100 ka cycle lags ice volume build-up by 280 ka. *Earth and Planetary Science Letters*, *151*(1–2), 117–123.

Norton, K., & Schlunegger, F. (2018). Migrating deformation in the Central Andes from enhanced orographic rainfall. *Nature Communications*, *2*, 584–7. https://doi.org/10.1038/ncomms1590

Omarini, R. H. (1983). *Caracterización Litológica, Diferencíon y Génesis de la Formación Puncoviscana entre el Valle de Lerma y la Faja Eruptiva de la Puna*, 244 p. Salta, Argentina: Universidad Nacional De Salta.

del Papa, C., Hongn, F., Powell, J., Payrola, P., Do Campo, M., Strecker, M. R., … Pereyra, R. (2013). Middle Eocene-Oligocene broken-foreland evolution in the Andean Calchaqui Valley, NW Argentina: Insights from stratigraphic, structural and provenance studies. *Basin Research*, *25*(5), 574–593. https://doi.org/10.1111/bre.12018

del Papa, C. E., & Petrinovic, I. A. (2017). The development of Miocene extensional and short-lived basin in the Andean broken foreland: The Conglomerado Los Patos, Northwestern Argentina. *Journal of South American Earth Sciences*, *73*, 191–201. https://doi.org/10.1016/j.jsames.2016.12.008

Payrola, P. A., Powell, J., del Papa, C. E., & Hongn, F. D. (2009). Middle Eocene deformation-sedimentation in the Luracatao Valley: Tracking the beginning of the foreland basin of northwestern Argentina. *Journal of South American Earth Sciences*, *28*(2), 142–154. https://doi.org/10.1016/j.jsames.2009.06.002

Pearson, D. M., Kapp, P. A., DeCelles, P. G., Reiners, P. W., Gehrels, G. E., Ducea, M. N., & Pullen, A. (2013). Influence of pre-Andean crustal structure on Cenozoic thrust belt kinematics and shortening magnitude: Northwestern Argentina. *Geosphere*, *9*(6), 1766–1782. https://doi.org/10.1130/GES00923.S2

Pearson, D. M., Kapp, P., Reiners, P. W., Gehrels, G. E., Ducea, M. N., Pullen, A., … Alonso, R. N. (2012). Major Miocene exhumation by fault-propagation folding within a metamorphosed, early Paleozoic thrust belt: Northwestern Argentina. *Tectonics*, *31*(4), 1–24. https://doi.org/10.1029/2011TC003043

Petrinovic, I. A., Marti, J., Aguirre-Díaz, G. J., Guzmán, S., Geyer, A., & Paz, N. S. (2010). The Cerro Aguas Calientes caldera, NW Argentina: An example of a tectonically controlled, polygenetic collapse caldera, and its regional significance. *Journal of Volcanology and Geothermal Research*, *194*(1–3), 15–26. https://doi.org/10.1016/j.jvolgeores.2010.04.012

Petrinovic, I. A., Mitjavila, J., Viramonte, J. G., Marti, J., Becchio, R., Arnosio, M., & Colombo, F. (1999). Descripción geoquímica y geocronológica de secuencias volcánicas neógenas de Trasarco, en el extremo oriental de la Cadena Volcánica Transversal del Que var (Noroeste de Ar gentina). *Acta Geologica Hispanica*, *34*(2–3), 255–272.

Petrinovic, I. A., Riller, U., Brod, J. A., Alvarado, G., & Arnosio, M. (2006). Bimodal volcanism in a tectonic transfer zone: Evidence for tectonically controlled magmatism in the southern Central Andes, NW Argentina. *Journal of Volcanology and Geothermal Research*, *152*(3–4), 240–252. https://doi.org/10.1016/j.jvolgeores.2005.10.008

Pingel, H., Alonso, R. N., Mulch, A., Rohrmann, A., Sudo, M., & Strecker, M. R. (2014). Pliocene orographic barrier uplift in the southern Central Andes. *Geology*, *42*(8), 691–694. https://doi.org/10.1130/G35538.1

Pingel, H., Mulch, A., Alonso, R. N., Cottle, J., Hynek, S. A., Poletti, J., … Strecker, M. R. (2016). Surface uplift and convective rainfall along the southern Central Andes (Angastaco Basin, NW Argentina). *Earth and Planetary Science Letters*, *440*, 33–42. https://doi.org/10.1016/j.epsl.2016.02.009

Pingel, H., Strecker, M. R., Alonso, R. N., & Schmitt, A. K. (2013). Neotectonic basin and landscape evolution in the Eastern Cordillera of NW Argentina, Humahuaca Basin (~24 S). *Basin Research*, *25*(5), 554–573. https://doi.org/10.1111/bre.12016

Ramos, V. A. (1970). *Geología de los primeros contrafuertes de la Puna saltojujeña entre San Antonio de los Cobres y el Moreno*. (J. C. M. Turner, Ed.). Doctoral Thesis., 86 p. Buenos Aires, Argentina: Universidad de Buenos Aires.

Ramos, V. A. (1973). Estructura de los primeros contrafuertes de la Puna salto-jujeña y sus manifestaciones volcánicas asociadas (Vol. 4, pp. 159–202). Presented at the 5th Congreso Geológico Argentino, Buenos Aires.

Schildgen, T. F., Robinson, R. A. J., Savi, S., Phillips, W. M., Spencer, J. Q. G., Bookhagen, B., … Strecker, M. R. (2016). Landscape response to late Pleistocene climate change in NW Argentina: Sediment flux modulated by basin geometry and connectivity. *Journal of Geophysical Research*, *121*(2), 392–414. https://doi.org/10.1002/2015JF003607

Schlunegger, F., Norton, K. P., & Zeilinger, G. (2011). Climatic forcing on channel profiles in the Eastern Cordillera of the Coroico Region. *Bolivia. Journal of Geology*, *119*(1), 97–107.

Schreiber, U., & Schwab, K. (1991). Geochemistry of quaternary shoshonitic lavas related to the Calama-Olacapato-El Toro Lineament, NW Argentina. *Journal of South American Earth Sciences*, *4*(1–2), 73–85. https://doi.org/10.1016/0895-9811(91)90019-H

Schwanghart, W., & Kuhn, N. J. (2010). TopoToolbox: A set of Matlab functions for topographic analysis. *Environmental Modelling and Software*, *25*(6), 770–781. https://doi.org/10.1016/j.envsoft.2009.12.002

Schwanghart, W., & Scherler, D. (2014). Short Communication: TopoToolbox 2 – MATLAB-based software for topographic analysis and modeling in Earth surface sciences. *Earth Surface Dynamics*, *2*(1), 1–7. https://doi.org/10.5194/esurf-2-1-2014

Seggiaro, R., Guzmán, S., Pereyra, R., Coppolecchia, M., & Cegarra, M. (2016). Neotectónica y volcanismo monogenético cuaternario sobre el segmento central del lineamiento Calama Olacapato Toro, NO Argentino. *Revista De La Asociación Geológica Argentina*, *73*(4), 468–477.

Sobel, E. R., Hilley, G. E., & Strecker, M. R. (2003). Formation of internally drained contractional basins by aridity-limited bedrock incision. *Journal of Geophysical Research*, *108*(B7), 2344. https://doi.org/10.1029/2002JB001883

Steinmetz, R. L., & Galli, C. I. (2015). Basin development at the eastern border of the Northern Puna and its relationship with the plateau evolution. *Journal of South American Earth Sciences*, *63*, 244–259. https://doi.org/10.1016/j.jsames.2015.07.017

Strecker, M. R., Alonso, R., Bookhagen, B., Carrapa, B., Coutand, I., Hain, M. P., & Sobel, E. R. (2009). Does the topographic distribution of the central Andean Puna Plateau result from climatic or geodynamic processes? *Geology*, *37*(7), 643–646. https://doi.org/10.1130/G25545A.1

Strecker, M. R., Alonso, R. N., Bookhagen, B., Carrapa, B., Hilley, G. E., Sobel, E. R., & Trauth, M. H. (2007). Tectonics and climate of the southern central Andes. *Annual Reviews in Earth and Planetary Sciences*, *35*, 747–787. https://doi.org/10.1146/annurev.earth.35.031306.140158

Streit, R. L., Burbank, D. W., Strecker, M. R., Alonso, R. N., Cottle, J. M., & Kylander Clark, A. R. C. (2015). Controls on intermontane basin filling, isolation and incision on the margin of the Puna Plateau, NW Argentina (~23°S). *Basin Research*, *29*(1), 131–155. https://doi.org/10.1111/bre.12141

Tchilinguirian, P., & Pereyra, F. X. (2001). Geomorfología del sector Salinas Grandes-Quebrada de Humahuaca, provincia de Jujuy. *Revista Asociación Geológica Argentina*, *56*, 3–15.

Tofelde, S., Schildgen, T. F., Savi, S., Pingel, H., Wickert, A. D., Bookhagen, B., … Strecker, M. R. (2017). 100 kyr fluvial cut-and-fill terrace cycles since the Middle Pleistocene in the southern Central Andes, NW Argentina. *Earth and Planetary Science Letters*, *473*, 141–153. https://doi.org/10.1016/j.epsl.2017.06.001

Turner, J. (1960). Estratigrafía de la Sierra de Santa Victoria y adyacencias. *Bol. Acad. Nac. De Ciencias Córdoba*, *41*(2), 163–196.

Vandervoort, D. S., Jordan, T. E., Zeitler, P., & Alonso, R. N. (1995). Chronology of internal drainage development and uplift, southern Puna plateau. *Argentine central Andes. Geology*, *23*(2), 145–148. https://doi.org/10.1130/0091-7613(1995) 023<0145:COIDDA>2.3.CO;2

Vermeesch, P. (2012). On the visualisation of detrital age distributions. *Chemical Geology*, *312-313*(C), 190–194. https://doi.org/10.1016/j.chemgeo.2012.04.021

Vezzoli, L., Acocella, V., Omarini, R., & Mazzuoli, R. (2012). Miocene sedimentation, volcanism and deformation in the Eastern Cordillera (24 30′ S, NW Argentina): tracking the evolution of the foreland basin of the Central Andes. *Basin Research*, *24*(6), 637–663.

Viramonte, J. G., Reynolds, J. H., del Papa, C. E., & Disalvo, A. (1994). The Corte Blanco garnetiferous tuff: A distinctive late Miocene marker bed in northwestern Argentina applied to magnetic polarity stratigraphy in the Río Yacones, Salta Province. *Earth Planet Sci Lett*, *121*, 519–531. https://doi.org/10.1016/0012-821X(94)90088-4

Vizy, E. K., & Cook, K. H. (2007). Relationship between Amazon and high Andes rainfall. *Journal of Geophysical Research*, *112*(D7), D07107. https://doi.org/10.1029/2006JD007980

Walker, R. T., Ramsey, L. A., & Jackson, J. (2011). Geomorphic evidence for ancestral drainage patterns in the Zagros Simple Folded Zone and growth of the Iranian plateau. *Geological Magazine*, *148*(5–6), 901–910. https://doi.org/10.1017/S0016756811000185

SUPPORTING INFORMATION

Additional supporting information may be found online in the Supporting Information section at the end of the article.

How to cite this article: Pingel H, Alonso RN, Altenberger U, Cottle J, Strecker MR. Miocene to Quaternary basin evolution at the southeastern Andean Plateau (Puna) margin (ca. 24°S lat, Northwestern Argentina). *Basin Res*. 2019;00:1–19. https://doi.org/10.1111/bre.12346